Lithic and mineral clasts in the Dar Al Gani (DAG) 319 polymict ureilite

Yukio Ikeda[1], M. Prinz[2] and C. E. Nehru[2]

[1]*Department of Materials and Biological Sciences, Ibaraki University, Mito 310–8512*
[2]*Department of Earth and Planetary Sciences, American Museum of Natural History, New York, NY 10024–5192, U.S.A.*

Abstract: Essentially all of the lithic and mineral clasts in DAG 319, a new polymict ureilite, were studied in order to determine their petrographic and mineralogical characteristics and their petrologic relationships to one another. Most of the clasts are identifiably from the ureilite parent body or appear to be shock-modified clasts from that body. Others appear to be projectiles derived from other bodies. The many kinds of lithic and mineral clasts found were classified into seven major groups, from A to G. The coarse-grained mafic lithic clasts (A) include three types of ureilitic lithology: type I ureilites, the predominant type, are similar to the common monomict ureilites; type II ureilites are a rare type with an olivine-orthopyroxene-augite lithology with essentially no carbon, and contain magmatic inclusions in the olivines and orthopyroxenes (similar to those in the Hughes 009 ureilite); a third type are magnesian ureilites with an mg >0.90, which are shock-produced. Fine-grained mafic lithic clasts (B) may have been derived from typical ureilites by shock, recrystallization, reduction, and/or melting. Felsic lithic clasts (C) are rare and important plagioclase-bearing igneous lithologies, which may represent the so-called missing basaltic melts separated during the formation of the ureilites. These represent several different lithic components. Dark clasts (D) consist mainly of phyllosilicates and sulfides, as well as magnetite (sometimes as framboidal clusters) and carbonates (dolomite, magnesite); some phyllosilicates occur as veins. Sulfide or metal-rich clasts (E) are shock-related, fine-grained lithologies to which sulfide and/or metal has been added; metal-rich clasts may have formed by reduction, and sulfide-rich clasts by oxidation. Rare chondrules and chondritic fragments (F) may be from projectiles which collided with the DAG 319 parent body, and they have characteristics that are more closely related to ordinary than to carbonaceous chondrites. Isolated mineral clasts (G) include many kinds of minerals produced by disaggregation of lithic clasts, but the origin of some of these minerals is uncertain. This paper describes all of these clasts, and is intended as a comprehensive study of the petrologic and mineralogical features of polymict ureilites. Such a description is a necessary prelude to a more complete understanding of the origin of the ureilitic meteorites.

1. Introduction

The Dar Al Gani (DAG) 319 meteorite is the newest polymict ureilite. It was recovered in the Libyan Desert in 1997 and weighed 740 g. Other polymict ureilites

that have been studied include Nilpena (Jaques and Fitzgerald, 1982; Prinz *et al.*, 1983; Brearley and Prinz, 1992), North Haig (Prinz *et al.*, 1986; Davis *et al.*, 1988), EET 83309 (Prinz *et al.*, 1987; Davis and Prinz, 1989), and EET 87720 (Warren and Kallemeyn, 1991). All of them are petrographically similar, although North Haig contains abundant mosaicized olivine, which is minor in the others.

The DAG 319 polymict ureilite is a complex breccia, which consists of a wide variety of lithic and mineral clasts, as do the other polymict ureilites. It is not clear whether or how most of the clasts are related to one another. Some may be various components of the same parent body, and others may be projectile materials. Clayton and Mayeda (1988) analyzed six chips of Nilpena; three whole rock, one ureilitic clast, one plagioclase-rich clast, and one dark inclusion, and all fell on or near the C3 line, indicating a possible relationship of some sort. But the petrologic and oxygen isotopic data of previous studies is limited.

Our goal in this paper is to carry out a thorough mineralogical and petrological study of essentially every lithic and mineral clast in DAG 319, and then classify these materials. Previous studies have examined the largest and most interesting clasts, but did not attempt to describe all of them. The present study of all clasts results in a rather complex classification scheme; yet even after this thorough examination it is still uncertain as to how some of the clasts are related. Thus, this paper is an essential first step in determining the nature of the lithic and mineral clasts in this complex breccia. Papers to follow include: (1) a study of the magmatic inclusions in the olivines and pyroxenes of one of the ureilite clasts (called type II in this paper) and in a large plagioclase clast, in order to determine the magmatic history of the melt components, (2) an oxygen isotopic study, with N. T. Kita, of some of the lithic and mineral clasts, using a Cameca 1270 ion microprobe; a preliminary report is in Kita *et al.* (1999), (3) a study of the petrogenesis of the ureilite parent body.

2. Analytical methods

Minerals and glasses were analyzed by an electron-probe micro-analyzer (EPMA) with a beam current of 3–10 nAmp, accelerating voltage of 15 kV and counting times of ten seconds. The detection limits for minor element contents of minerals are about 0.05 wt% for Al_2O_3, 0.1 wt% for TiO_2, Cr_2O_3, CaO, Na_2O, and K_2O, and 0.2 wt% for MnO. The corrections were performed by the Bence and Albee method for silicates and oxides and by the standard ZAF method for metal and sulfides. Glass was analyzed using a focussed beam of 3 nAmp for small glasses or a defocused beam with 3 nAmp for large glasses, about 5 μm across, in order to suppress evaporation of alkalis.

3. Sample description

Six thin sections of DAG 319 were studied, and their numbers are 4963-1, 4963-2, 4963-3, 4962-2, 4955-1, and 4963-4. These sections are designated as α, β, γ, δ,

ε, and ζ for simplicity in this study.

Thin section 4963-1 (α) contains many types of clasts but no large ureilitic clasts. Instead, it contains a large (5 mm) plagioclase fragment (G3-2, Table 1) which has many magmatic inclusions. Thin section 4963-2 (β) includes the same plagioclase fragment with magmatic inclusions as that in 4963-1 (α). The thin section was made from the same chip as 4963-1 (α), and the two sections are very similar.

Thin section 4963-3 (γ) contains a large lithic clast of an olivine-ortho-pyroxene-augite ureilite, which occupies 1/3 of the section. Thin section 4963-4 (ζ) also contains the same lithic clast of this unusual ureilite type. This section was made from the same chip as thin section 4963-3 (γ) and the two are very similar.

Thin section 4962-2 (δ) contains two large mafic lithic clasts, a fine-grained olivine-pyroxene clast and a coarse-grained clast of common monomict ureilite. The two clasts occupy about half the area of the section. Thin section 4955-1 (ε) differs in appearance from the other five thin sections, and has a large coarse-grained mafic lithic clast of common ureilite type which occupies more than 90% of the section.

4. Classification of clasts

Our classification of the clasts in DAG 319 is presented in Table 1. In consolidating all of the data, our goal was simplification wherever possible. Nevertheless, the complex nature of the materials required that a lengthy classification was utilized. The clasts are divided into seven broad groupings: Coarse-grained Mafic Lithic Clasts (A), Fine-grained Mafic Lithic Clasts (B), Felsic Lithic Clasts (C), Dark Clasts (D), Sulfide-rich or Metal-rich Clasts (E), Chondrules and Chondritic Fragments (F), and Isolated Mineral Clasts (G).

4.1. Coarse-grained mafic lithic clasts (A)

Coarse-grained mafic lithic clasts are the major lithic clast group of DAG 319, and the lithic clasts are sometimes large, more than 1 cm across. This group consists of three types: (A1) typical olivine (Ol)-pigeonite (Pig)-carbon ureilitic clasts, (A2) unusual Ol-orthopyroxene (Opx)-augite (Aug) ureilitic clasts, and (A3) magnesian ureilitic clasts. Representative compositions of minerals in these clasts are shown in Tables 2a, b.

Clasts of type A1 have an assemblage of olivine (Fo_{74-84}) and pigeonite, with carbon along their margins and in fractures. This type is common in DAG 319 (Figs. 1a, b) and they are designated type I ureilites. Type I ureilites show reduction of olivine up to forsterite ($Fo_{>95}$), a few tens of microns across, along grain margins and along fractures. This reverse zoning was caused by reduction during or after the consolidation of the type I ureilitic clasts with their associated carbon. They contain pigeonite similar in composition and occurrence to that in typical monomict ureilites (Goodrich, 1992), as well as Si-bearing kamacite with 8–12% Si, and sulfides. They are similar in mineralogy and texture to the common monomict ureilites.

Table 1.   Classification of lithic and mineral clasts in the DAG 319 polymict ureilite.

(A) Coarse-grained Mafic Lithic Clasts
  (A1) Ol-Pig ureilitic clasts, mg of core Ol=74–84 (type I)
  (A2) Ol-Opx-Aug ureilitic clasts, with mg of core Ol=85–90 (type II)
  (A3) Magnesian Ol-rich clasts, with minor Opx, mg of core Ol=91–98
(B) Fine-grained Mafic Lithic Clasts
  (B1) Magnesian Ol-Pyx type, mg of Ol=91–99
  (B2) Pyx-rich type, mg of Opx=83–99
  (B3) Fo-rich clasts, mg of Ol>95
  (B4) Granular Ol-rich type, with Opx (or Pig) and alkali-free glass,
        mg of Ol=74–84 (Normal zoning)
(C) Felsic Lithic Clasts
  (C1) Porphyritic type, An=1–60
  (C2) Pilotaxitic type: An=30–55
  (C3) Glassy clasts
      (C3-1) Magnesian glassy type, with En and Di, mg of En>95
      (C3-2) Ferroan glassy type, having CaO-rich comp., mg of Opx=55–80
  (C4) Gabbroic types
      (C4-1) Troctolitic type, with mg of Ol=93 and An=81
      (C4-2) Calcic Pl-Aug clasts, An>90
(D) Dark Clasts: phyllosilicates with mg=50–85
  (D1) Fa-free type, with anhydrous exotic fragments
  (D2) Fa-bearing type, with igneous fragments
(E) Sulfide or Metal-rich Lithic Clasts
  (E1) Sulfide-rich type, mg of Ol=47–83
  (E2) Metal-rich type, mg of En>98, or minor silica
(F) Chondrule and Chondrite Fragments
  (F1) Chondrules
      (F1-1) Barred Ol chondrule, mg of Ol=71
      (F1-2) Porphyritic Ol chondrule, mg of Ol=72–96 (Normal zoning)
      (F1-3) Porphyritic Ol-Opx chondrule, mg of Ol=82
      (F1-4) Porphyritic En-Di chondrule, mg of En=92–99 (Normal zoning)
      (F1-5) Radial-Pyx chondrules, mg of Opx=98–99
  (F2) Chondrites, with Ol, Opx, and Ab, mg of Ol=60–85
(G) Isolated Mineral Clasts (single crystal predominant)
  (G1) Olivines
      (G1-1) Ureilitic olivine (73<mg<99, sometimes mosaicized)
      (G1-2) Ferroan olivine (mg<72)
      (G1-3) Forsterite (mg>99)
  (G2) Pyroxenes
      (G2-1) Orthopyroxene (76<mg<98, mg of ferroan type <70)
      (G2-2) Pigeonite (76<mg<92, mg of ferroan type <70)
      (G2-3) Inverted pigeonite (pigeonite-orthopyroxene)
      (G2-4) Enstatite (mg>99)
      (G2-5) Augite (or diopside)
      (G2-6) Fassaite (Al_2O_3 >5 wt%)
  (G3) Plagioclases
      (G3-1) Calcic plagioclase (An>80)
      (G3-2) Intermediate plagioclase (40<An<70).
              A large Pl fragment contains magmatic inclusions
      (G3-3) Sodic plagioclase, An<40

Table 1.   (Continued).

(G4)	Chromites	
(G5)	Ilmenites	
(G6)	Phosphates	
	(G6-1)	Apatite
	(G6-2)	Whitlockite
(G7)	Bladed graphites	
(G8)	Sulfides	
	(G8-1)	Troilite (or pyrrhotite)
	(G8-2)	Pentlandite
(G9)	Metal	
	(G9-1)	Kamacite with $Ni = 1\text{-}6$ wt% and Si of $1\text{-}13$ wt%
	(G9-2)	Silicide: Suessite and Perryite
	(G9-3)	Phosphide: Schreibersite and Barringerite
	(G9-4)	Taenite: Ni wt% up to 28 wt%

The mg ratios are 100 times larger than those in the text.

Clasts of type A2 are Ol-Opx-Aug assemblages with essentially no carbon (Figs. 1c, d), and are designated type II ureilites. The cores of the olivine are almost homogeneous (Fo_{86-89}) with no reduction along olivine grain margins. Pyroxenes are orthopyroxene and augite, similar in composition and occurrence to those in the unusual monomict ureilites Hughes 009 and FRO 90054 (Tribaudino *et al.*, 1997, Goodrich *et al.*, 1999a, b). They contain Si-poor kamacite ($<0.1\%$ Si) and schreibersite, as well as sulfides. Most importantly, type II ureilites have melt inclusions in their olivines and orthopyroxenes. The largest clast (ζ1) is 1 cm across; it has experienced slight reduction, and enstatite occurs rarely on rims of olivine.

Magnesian ureilitic clasts (A3) consist mainly of olivine with Fo_{90-98}, with minor amounts of orthopyroxene and diopside. The olivines have remarkable reverse zoning up to Fo_{99}. Two magnesian ureilitic clasts are shown in Figs. 1e, f.

4.2.   Fine-grained mafic lithic clasts (B)

Fine-grained mafic lithic clast group (B) includes four types (B1-4), and representative chemical compositions of minerals in these clasts are shown in Tables 3a, b. The magnesian Ol-pyroxene (Pyx) clasts (B1, Figs. 2a–d) consist mainly of magnesian olivine with $Fo_{>91}$ and pyroxenes which are orthopyroxene, pigeonite and augite. An aggregate of small olivine grains in this type seems to correspond to an original large olivine grain (Fig. 2b), and an aggregate of small pyroxene grains seem to correspond to an original large pyroxene grain of ureilitic lithology (Fig. 2d). This type may have experienced shock, recrystallization, and reduction of typical monomict ureilites to produce their fine-grained nature.

Fine-grained Pyx-rich type (B2, Figs. 2e, f) consists mainly of fine-grained pyroxene aggregates, where the pyroxenes are orthopyroxene, pigeonite, and augite. The texture (Fig. 2e) of this type suggests that original pigeonite was replaced by fine-grained orthopyroxene and augite with minor SiO_2-rich glass (Table 3a), and this replacement is common in monomict ureilites (Berkley *et al.*, 1980; Ikeda,

Table 2a. Chemical compositions of silicate minerals in coarse-grained mafic (ureilite) lithic clasts (group A).

Type	A1	A1	A1	A1	A1	A1	A1	A1	A1	A1	A1	A1	A2	A2	A2	A2	A2	A2
Clast	ε1	ε1	ε1	ε1	δ3	δ3	δ3	δ3	δ2	δ2	δ2	δ2	γ1	γ1	γ1	γ1	γ1	γ1
No.	2	4	16	20	288	282	274	275	15	16	13	22	18	24	6	3	30	32
Mineral	Ol	Ol	Pig	Pig	Ol	Ol	Pig	Pig	Ol	Ol	Pig	Pig	Ol	Ol	Opx	Opx	Aug	Aug
SiO2	38.18	38.29	54.83	54.85	38.40	38.09	54.52	54.56	38.00	38.60	53.78	55.60	40.35	40.32	57.13	56.75	54.30	53.60
TiO2	0.00	0.00	0.00	0.03	0.00	0.00	0.00	0.03	0.00	0.00	0.00	0.00	0.00	0.00	0.02	0.04	0.24	0.25
Al2O3	0.00	0.00	0.73	0.68	0.00	0.00	0.63	0.55	0.04	0.00	0.43	0.47	0.00	0.00	1.01	0.86	1.72	1.42
Cr2O3	0.46	0.59	1.06	1.07	0.69	0.65	1.28	1.17	0.97	0.67	1.07	1.08	0.48	0.48	0.91	1.08	1.18	1.37
FeO	19.46	19.90	11.42	12.25	22.09	21.81	13.00	12.98	20.12	19.09	11.80	11.13	11.07	11.68	6.96	6.91	4.14	3.91
MnO	0.43	0.46	0.34	0.32	0.38	0.59	0.16	0.35	0.63	0.64	0.74	0.43	0.64	0.46	0.67	0.55	0.51	0.20
MgO	40.22	40.31	26.43	25.98	38.65	38.81	26.58	25.77	40.00	40.54	27.36	26.23	47.03	47.12	31.38	31.05	19.75	19.71
CaO	0.31	0.32	4.45	4.51	0.34	0.35	3.54	3.52	0.47	0.24	4.66	4.27	0.27	0.26	2.67	2.48	18.65	18.18
Na2O	0.00	0.00	0.04	0.07	0.00	0.00	0.05	0.05	0.00	0.00	0.00	0.03	0.00	0.04	0.14	0.14	0.37	0.33
K2O	0.02	0.03	0.00	0.00	0.00	0.00	0.00	0.00	0.00	0.00	0.00	0.01	0.00	0.00	0.00	0.00	0.00	0.00
Total	99.08	99.90	99.30	99.76	100.55	100.30	99.76	98.98	100.23	99.78	99.84	99.25	99.84	100.36	100.89	99.86	100.86	98.97
mg ratios	0.79	0.78	0.80	0.79	0.76	0.76	0.78	0.78	0.78	0.79	0.81	0.81	0.88	0.88	0.89	0.89	0.89	0.90

Type	A3	A3	A3	A3	A3	A3	A3	A3	A3	A3
Clast	α10A	α10A	α10A	α10A	α10A	α10A	α37A	α37A	α37A	α37A
No.	635	636	626	629	1395	1403	1165	1922	1167	1923
Mineral	Ol	Ol	Ol	Opx	Opx	Aug	Ol	Ol	Opx	Opx
SiO2	41.33	41.81	43.13	57.70	57.71	54.54	41.68	41.87	58.29	58.04
TiO2	0.00	0.00	0.00	0.07	0.12	0.62	0.00	0.02	0.13	0.16
Al2O3	0.00	0.00	0.04	0.96	0.95	2.81	0.00	0.00	0.38	0.45
Cr2O3	0.25	0.29	0.05	0.37	0.45	0.61	0.45	0.45	0.65	0.62
FeO	8.09	6.18	0.34	4.75	5.87	1.24	3.63	2.63	1.55	2.26
MnO	0.24	0.20	0.08	0.18	0.16	0.20	0.16	0.33	0.29	0.41
MgO	49.21	51.42	56.96	33.53	33.90	20.66	53.75	53.72	34.87	33.31
CaO	0.25	0.24	0.21	2.17	2.15	20.32	0.33	0.34	2.58	2.69
Na2O	0.01	0.00	0.00	0.00	0.02	0.34	0.10	0.00	0.13	0.09
K2O	0.00	0.00	0.00	0.00	0.00	0.01	0.00		0.06	0.00
Total	99.38	100.14	100.81	99.73	101.33	101.35	100.10	99.36	98.93	98.03
mg ratios	0.92	0.94	1.00	0.93	0.91	0.97	0.96	0.97	0.98	0.96

Table 2b. *Chemical compositions of metal and sulfide in coarse-grained mafic (ureilite) lithic clasts (group A).*

Type	A1	A1	A1	A1	A1	A1	A1	A1	A1	A1	A1	A1	A1	A1
Clast	$\varepsilon 1$	$\varepsilon 1$	$\varepsilon 1$	$\varepsilon 1$	$\varepsilon 1$	$\delta 3$	$\delta 3$	$\delta 3$	$\delta 3$	$\delta 2$	$\delta 2$	$\delta 2$	$\delta 2$	$\delta 2$
No.	M13	M23	M29	M6	M5	M63	M64	M102	M103	M79	M80	M95	M96	M99
Mineral	Ka	Ka	Ka	Sulfide	Sulfide	Ka	Ka	Sulfide	Sulfide	Ka	Ka	Sulfide	Sulfide	Sulfide
Si	8.92	9.35	10.12	0.03	0.04	10.62	10.44	0.01	0.03	0.04	0.03	0.00	0.00	0.03
P	0.31	0.29	0.24	0.00	0.00	0.29	0.28	0.00	0.00	0.06	0.08	0.00	0.00	0.00
S	0.03	0.00	0.00	36.84	36.62	0.02	0.00	36.70	36.70	0.00	0.01	36.41	35.86	35.94
Cr	0.12	0.11	0.15	1.27	1.34			0.38	0.37			0.00	0.09	0.03
Mn	0.02	0.00	0.00	0.08	0.12			0.02	0.08			0.00	0.05	0.00
Fe	84.38	84.88	84.23	59.28	58.93	85.13	84.62	61.16	60.73	95.23	94.62	61.23	61.81	60.57
Co	0.39	0.38	0.40	0.09	0.11	0.28	0.35	0.08	0.05	0.19	0.26	0.11	0.17	0.15
Ni	3.99	3.97	3.69	0.17	0.19	4.59	4.55	0.14	0.13	2.48	2.37	1.27	0.53	1.80
Total	98.16	98.98	98.83	97.76	97.35	100.93	100.24	98.49	98.09	98.00	97.37	99.02	98.51	98.52

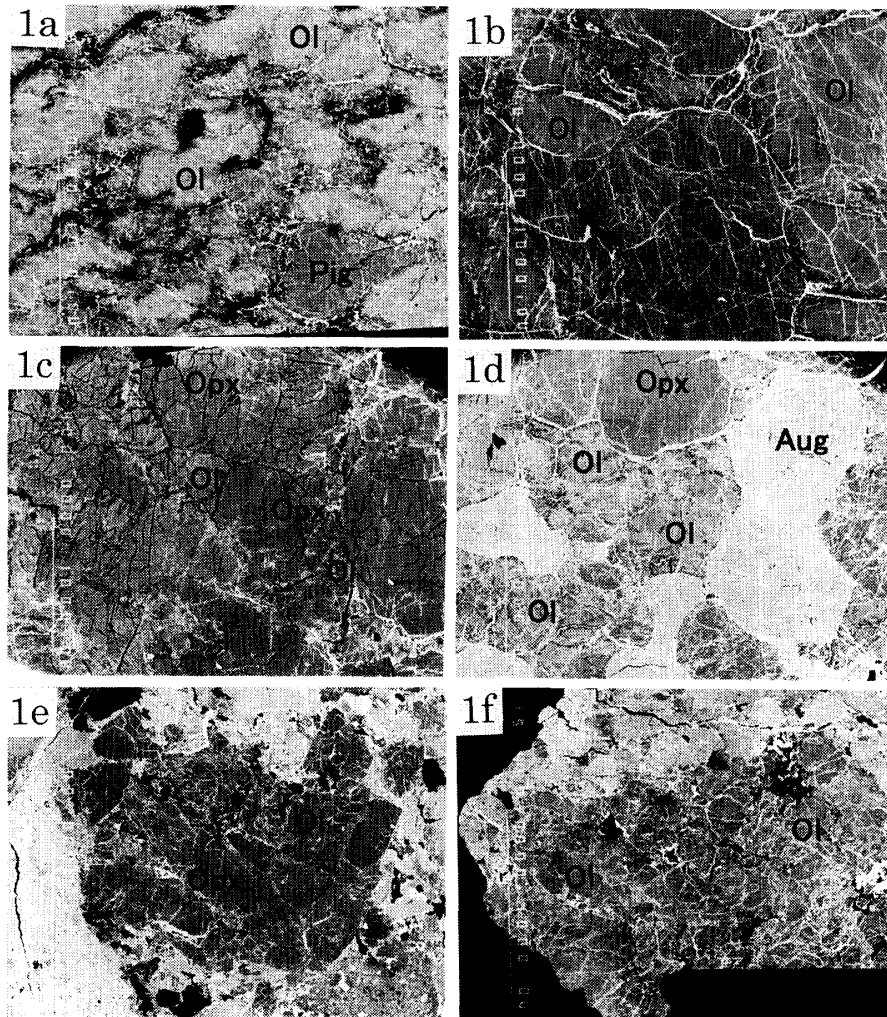| Type	A2	A2	A2	A2	A2
Clast	$\gamma 1$	$\gamma 1$	$\gamma 1$	$\gamma 1$	$\gamma 1$
No.	M7	M9	M95	M78	M81
Mineral	Ka	Schreib	Ka	Sulfide	Sulfide
Si	0.04	0.00	0.14	0.01	0.02
P	0.29	14.32	0.44	0.00	0.00
S	0.03	0.21	0.00	37.29	37.47
Cr			0.08	3.41	0.24
Mn			0.00	0.20	0.11
Fe	92.87	81.76	97.60	59.05	62.59
Co	0.41	0.22	0.13	0.00	0.11
Ni	4.53	2.35	1.33	0.00	0.00
Total	98.17	98.86	99.72	99.96	100.54

Fig. 1. Back scattered electron images of coarse-grained mafic (ureilitic) lithic clasts in the DAG
319 polymict ureilite. Symbols in parentheses after clast numbers correspond to groups in
Table 1.

(a) Clast δ3 (A1) is a typical type I monomict ureilitic clast, consisting mainly of olivine (core;
Fo_{75-76}) and pigeonite, with dark carbon and metal. Note that the rims of the olivine grains
are magnesian due to reduction. Width, about 2.6 mm.

(b) Clast ε1 (A1) is a type I monomict ureilitic clast, consisting mainly of olivine (core; Fo_{77-79})
and pigeonite, with a metal-rich network and dark carbon. The rims of the olivine grains
experienced reduction. Width, about 2.6 mm.

(c) Clast γ1 (A2) is a type II ureilitic clast, consisting mainly of olivine (core; Fo_{86-88}),
orthopyroxene, and augite. Sometimes the olivine and orthopyroxene grains contain
magmatic inclusions about 100 microns across. Note the near absence of carbon. Width,
about 3 mm.

(d) Another image of clast γ1 (A2) with augite grains. Width, about 3 mm.

(e) Clast α37A (A3) is a magnesian ureilitic clast, consisting mainly of olivine (Fo_{96-97}) and
orthopyroxene. Width, about 3 mm.

(f) Clast α10A (A3) is a shocked magnesian ureilitic clast, consisting mainly of olivine (Fo_{91-95})
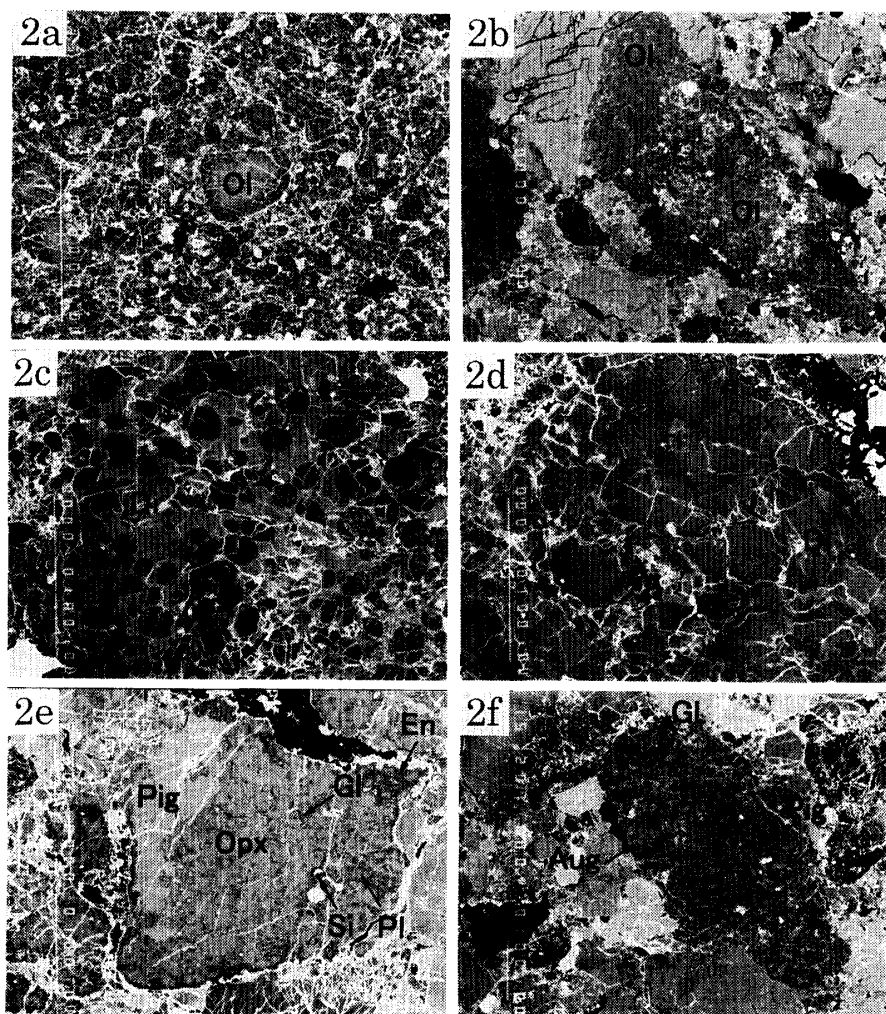with magnesian olivine rims up to Fo_{99}. Width, about 3 mm.

Fig. 2.   Back scattered electron images of fine-grained mafic lithic clasts.   Symbols in parentheses after clast numbers correspond to groups in Table 1.

(a)   Clast δ1 (B1) is a fine-grained mafic lithic clast, consisting mainly of typical ureilitic olivine (cores; Fo_{77}) and magnesian olivine (up to Fo_{99}) with minor amounts of pyroxene and sodic plagioclase. Width, about 2.7 mm.

(b)   Clast α35B (B1) is a heterogeneous fine-grained mafic lithic clast consisting of fine-grained olivine (Fo_{91}, upper left denoted by Ol), fine-grained pyroxene and olivine (middle portion denoted by Ol) and fine-grained pyroxene (lower right). Width, about 2.1 mm.

(c)   An enlarged image of the middle portion of clast α35B (B1), consisting of rounded olivine grains (Fo_{95-97}) poikilitically enclosed by diopside. Width, about 260 μ.

(d)   An enlarged image of the lower left portion of clast α35B (B1), consisting of reversely zoned orthopyroxene grains with interstitial diopside and a silica mineral. Width, about 270 μ.

(e)   Clast α33A (B2) is a fine-grained mafic lithic clast, consisting of a ureilitic pigeonite grain and a fine-grained aggregate of orthopyroxene, augite, plagioclase, and glass, with minor metal. Width, about 270 μ.

(f)   Clast α7C (B2) is a fine-grained mafic lithic clast, consisting of pigeonite, augite, orthopyroxene, and glass. Width, about 600 μ.
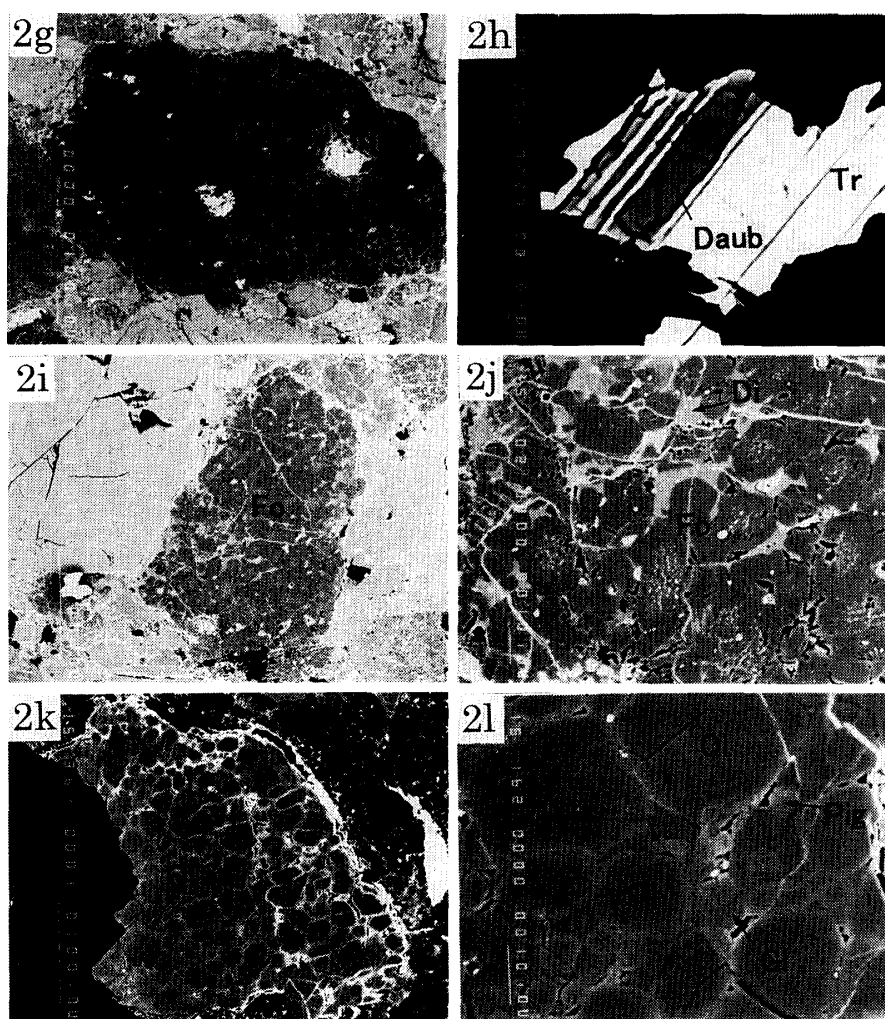
Fig. 2.   *(Continued).*

(g)   Clast $\alpha30$ *(B2) is a fine-grained clast, consisting of enstatite and sulfide-metal aggregates. The enstatite is* En_{99} *with low CaO. Width, about 1.2 mm.*

(h)   An enlarged image of a sulfide grain in the central portion of clast $\alpha30$ (B2). It consists of *troilite with daubreelite lamellae. Width, about 60 μ.*

(i)   Clast $\alpha32B$ *(B3) is a fine-grained clast consisting mainly of magnesian olivine* (Fo_{99}). *Width, about 400 μ.*

(j)   An enlarged image of the lower central portion of clast $\alpha32B$ (B3), showing forsterite with *minor diopside. Reduced olivine occurs in the cores of olivine grains and has tiny metal. Width, about 120 μ.*

(k)   Clast $\alpha8B$ *(B4) is a granular olivine clast, consisting mainly of olivine grains* (Fo_{78-81}). *Width, about 320 μ.*

(l)   An enlarged image of the lower central portion of clast $\alpha8B$ (B4), showing an igneous *texture. Interstitial phases are pigeonite and glass, which is almost alkali-free and has a composition similar to orthopyroxene. Width, about 70 μ.*

1999). The magnesian Ol-Pyx type (B1) often contains Pyx-rich portions similar in texture to that of the Pyx-rich clasts (B2), suggesting that the predominant fine-grained mafic lithic clasts (B1, B2) may have been derived from common monomict ureilites by shock, recrystallization, and reduction. Some fine-grained
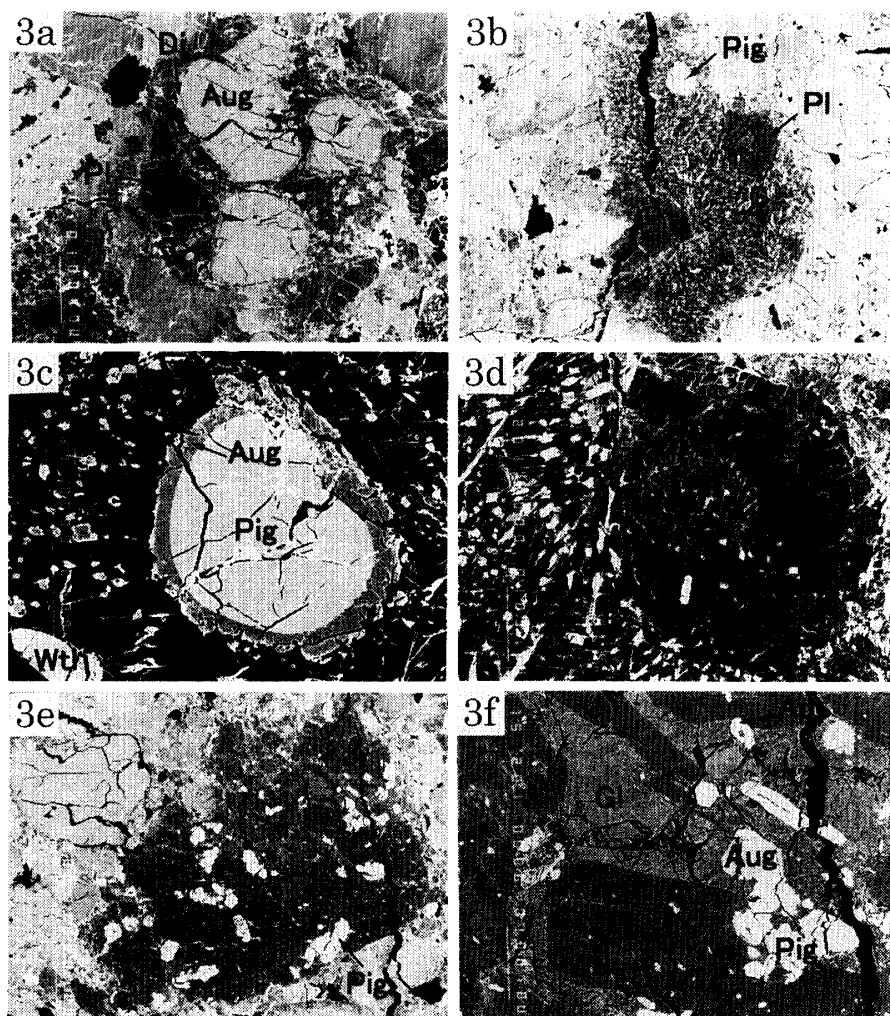
Fig 3. Back scattered electron images of felsic lithic clasts. Symbols in parentheses after clast numbers correspond to groups in Table 1.

(a) Clast α13 (C1) is a porphyritic felsic clast. Phenocrysts are augite and plagioclase, and there is interstitial groundmass between them. Phenocrysts of augite are surrounded by diopside rims, showing that reduction took place during crystallization after the phenocrysts of augite and prior to the diopside rims. Width, about 650 μ.

(b) Clast α34 (C1) is a porphyritic felsic clast consisting of phenocrysts of pigeonite and plagioclase, with a groundmass that consists mainly of sodic plagioclase and augite with minor whitlockite. Width, about 2.6 mm.

(c) An enlarged image of a pigeonite phenocryst in clast α34 (C1), showing that an augite rim surrounds the pigeonite phenocryst, and the augite rim is more magnesian than the pigeonite core. Width, about 300 μ.

(d) An enlarged image of a phenocryst of plagioclase in clast α34 (C1). Core plagioclase (An_{7-9}) is surrounded by mantle plagioclase (An_{21-4}). The inside rims are calcic (An_{19-21}) and the outermost rims are sodic (An_{4-6}), showing normal zoning in the rims. The plagioclase core contains a rounded island of plagioclase (An_{11-15}) which is the same composition as the phenocryst rims. The minor phases (whitish in the image) included in the plagioclase phenocryst are augite and whitlockite. Width, about 600 μ.

(e) Clast γ15 (C1) is a porphyritic felsic clast, consisting of phenocrysts of pigeonite and plagioclase with minor groundmass. The pigeonite phenocrysts sometimes show zoning from pigeonite to augite. Width, about 2.6 mm.
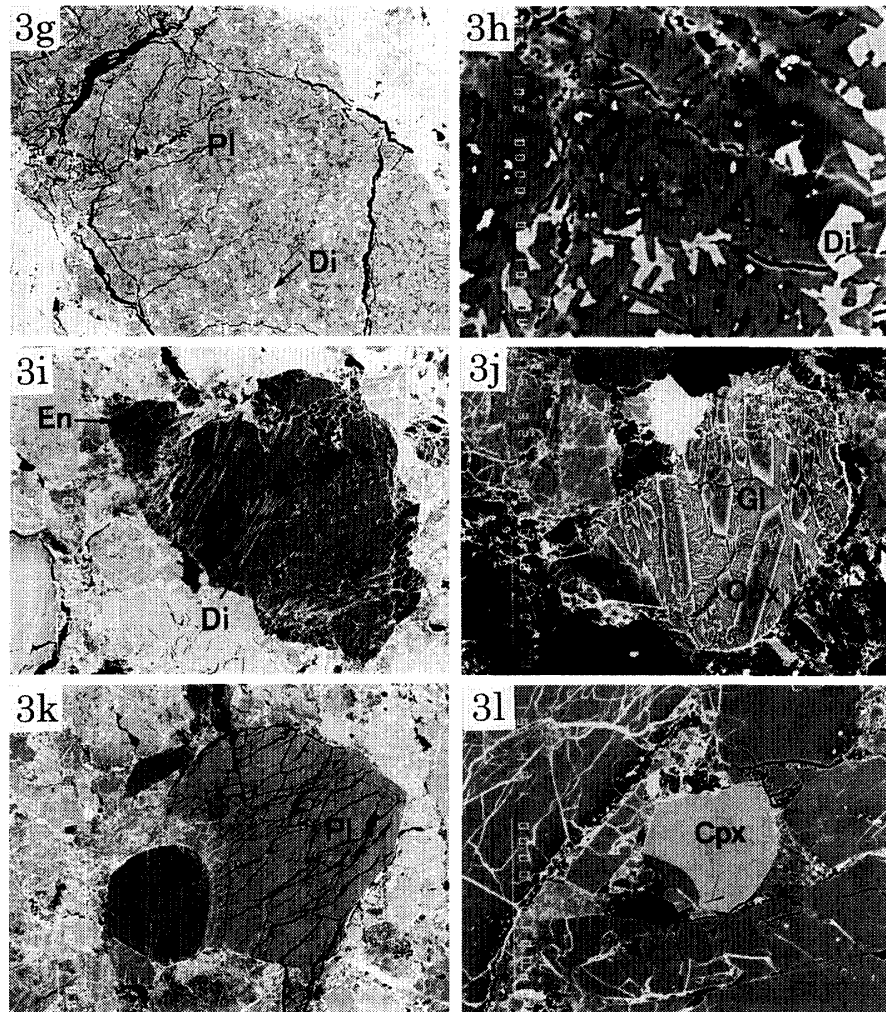
Fig. 3.   (Continued).

(f) An enlarged image of the upper right portion of clast $\gamma15$ (C1).   Plagioclase phenocrysts show normal zoning (An$_{9-2}$), and sometimes include pigeonite and whitlockite.   The groundmass consists of rhyolitic glass and augite needles, and includes microphenocrysts of apatite. Width, about 600 μ.

(g) Clast $\alpha24B$ (C2) is a pilotaxitic felsic clast consisting mainly of plagioclase laths with minor diopside grains. Width, about 400 μ.

(h) An enlarged image of clast $\alpha24B$ (C2), consisting of normally zoned plagioclase laths (An$_{54-30}$) and pigeonite-augite grains.   The interstitial mesostasis consists of feldspathic materials (An$_{20-2}$) and minor silica mineral. Width, about 120 μ.

(i) Clast $\alpha8A$ (C3-1) is a magnesian glassy felsic clast, consisting of rhyolitic glass with phenocrysts of enstatite and needle-like diopside. Width, about 1 mm.

(j) Clast $\alpha16A$ (C3-2 is a ferroan glassy felsic clast, including olivine and orthopyroxene.   The glass is enriched in CaO, poor in alkalis, and contains augite feather crystals.   The orthopyroxene crystals show chemical zoning from low-CaO orthopyroxene to high-CaO pigeonite. Width, about 370 μ.

(k) Clast $\gamma8$ (C4-1) is a troctolitic felsic clast consisting of calcic plagioclase (An$_{87-89}$) and olivine (Fo$_{93-94}$). Width, about 1.3 mm.

(l) Clast $\alpha21B$ (C4-2) has fassaitic clinopyroxene and minor plagioclase (An$_{99}$). Width, about 260 μ.
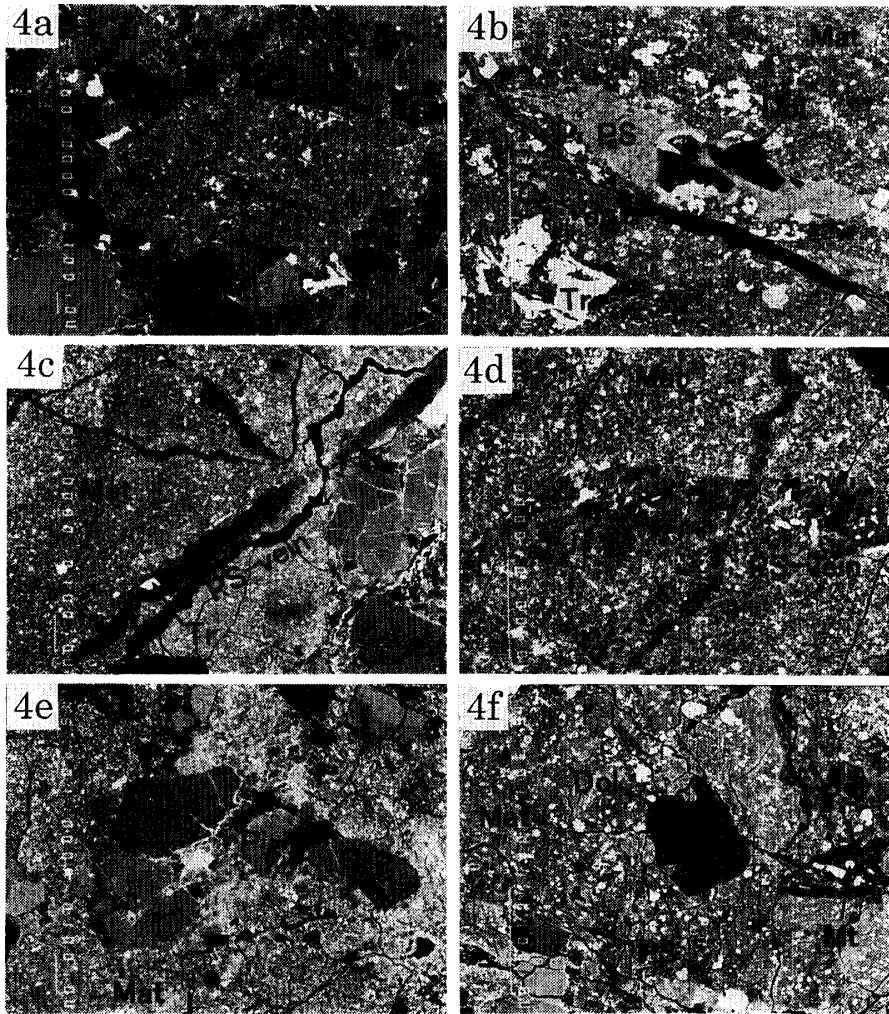
Fig. 4. *Back scattered electron images of dark clasts. Symbols in parentheses after clast numbers correspond to groups in Table 1.*

(a) *Clast α25A (D1) is a dark clast which is similar to dark inclusions in some carbonaceous chondrites. Width, about 2 mm.*

(b) *An enlarged image of the central portion of clast α25A (D1). Phyllosilicate vein occurs set in the matrix, and includes dolomite grains. Sulfide and magnetite occurs in the matrix and in the veins. Calcite veins are terrestrial weathering products. Width, about 260 μ.*

(c) *Clast δ5 (D1) is a dark clast, containing phyllosilicate veins in the matrix. Sometimes the veins include sulfide grains. Width, about 1.2 mm.*

(d) *Clast δ5 (D1) showing a broad phyllosilicate vein cut by a narrow phyllosilicate vein. Width, about 400 μ.*

(e) *Clast γ3 (D1) is a dark clast which includes anhydrous minerals such as olivine, pigeonite, and rhyolitic glass. Width, about 1.2 mm.*

(f) *The matrix of clast γ3 (D1) includes dolomite and phyllosilicate fragments, and aggregates of phyllosilicates, magnetite, and sulfide. Width, about 400 μ.*

Pyx-rich clasts consist mainly of enstatite (Fig. 2g), and these contain daubreelite (Fig. 2h).

Rare plagioclase grains in fine-grained Ol-Pyx (B1) and Pyx-rich (B2) types are An_9 and An_{85}, respectively (Table 3a). Glasses also occur in the interstitial
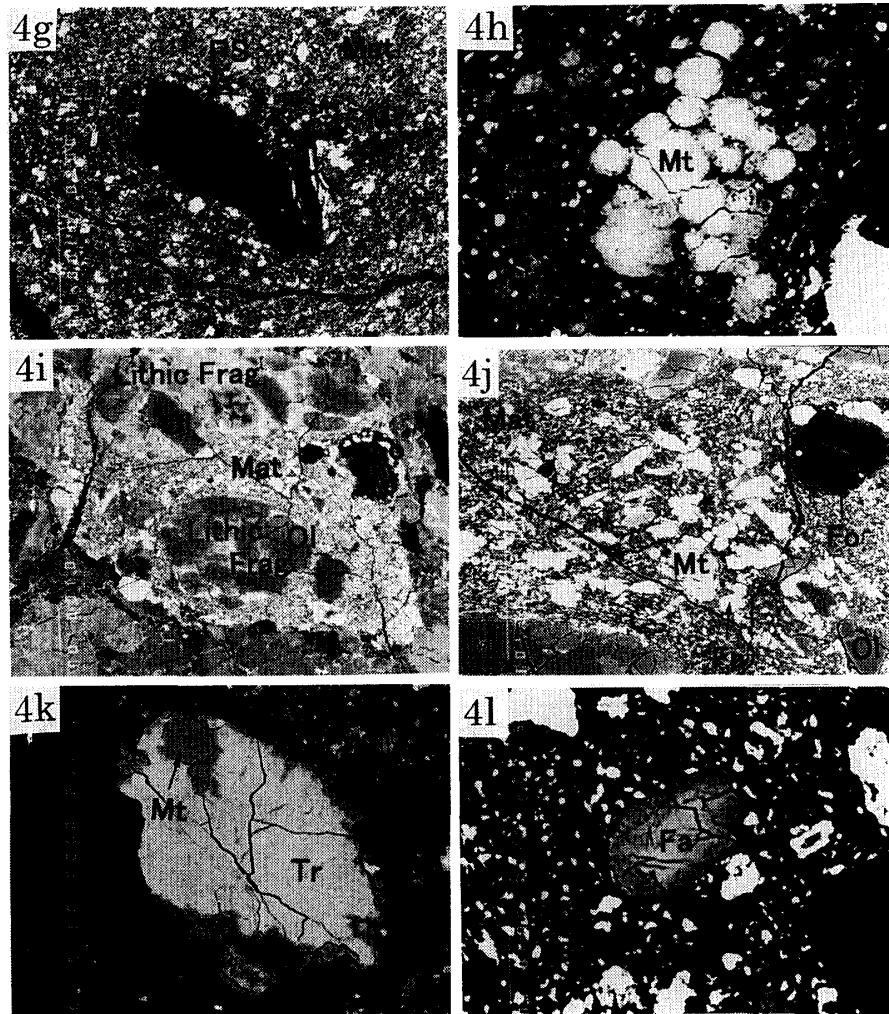
Fig. 4.   (Continued).

(g)   Clast δ6 (D1) includes phyllosilicate fragments and magnetite.   Width, about 400 μ.

(h)   The matrix of clast δ6 (D1) includes framboidal magnetite.   Width, about 95 μ.

(i)   Clast α27 (D2) is a fayalite-bearing phyllosilicate-rich clast.   This clast includes a few igneous fragments (Lithic Frag) consisting of magnesian olivine and orthopyroxene with groundmass, where the olivine has normal zoning (Fo_{99-75}), and the groundmass is hydrated as phyllosilicates.   The matrix between the igneous clasts consists mainly of phyllosilicates and magnetite, including magnesian olivine grains (Fo).   Width, about 1 mm.

(j)   An enlarged image of the matrix of clast α27 (D2).   The matrix includes magnesian olivine grains of Fo_{99}, and the boundary between the magnesian olivine and the matrix is very sharp.   Width, about 240 μ.

(k)   An enlarged image of sulfide in clast α27 (D2).   The sulfide grain is surrounded by magnetite, suggesting that the magnetite was produced from sulfide.   Width, about 120 μ.

(l)   An enlarged image of the matrix of clast α27 (D2).   Fayalite grains in the matrix have reverse zoning Fo_{1-26}.   Width, about 56 μ.

spaces of these types (B1, B2). They are rich in SiO_2 and feldspathic components, and very similar to glasses in common monomict ureilites (Ikeda, 1999).   Silica minerals are rare and occur in these types (B1, B2).

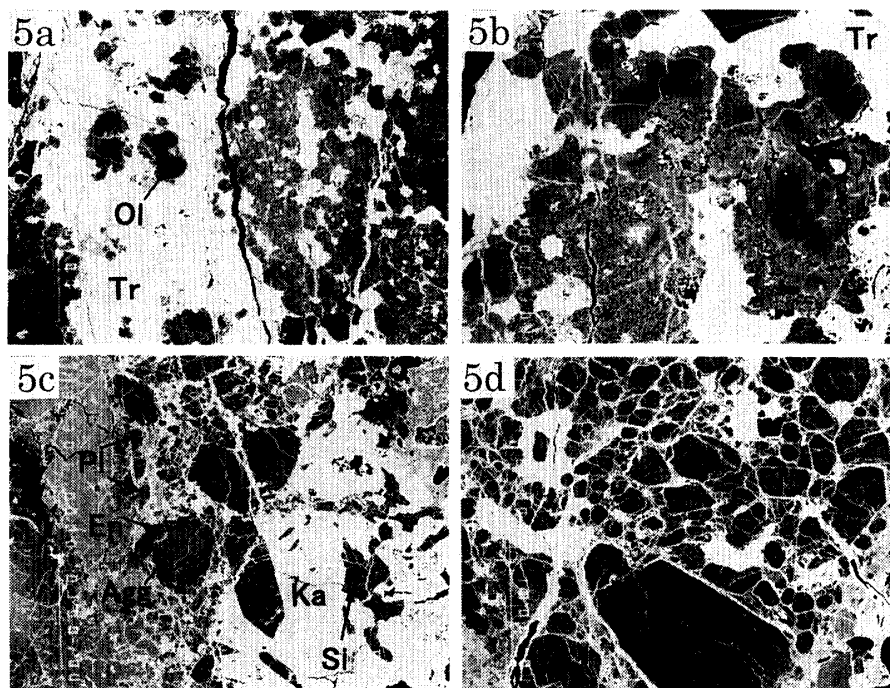Fine-grained forsterite (Fo)-rich clasts (B3) are aggregates of magnesian

Fig. 5. Back scattered electron images of sulfide- or metal-rich clasts. Symbols in parentheses
after clast numbers correspond to groups in Table 1.

(a) Clast α32A (E1) is a sulfide-rich clast consisting mainly of sulfide and olivine. Width,
about 600 μ.

(b) An enlarged image of the upper central portion of Clast α32A (E1). The olivine grains have
normal zoning, from Fo_{83-47}, and the matrix-like portion is porous. Width, about 170 μ.

(c) Clast α42 (E2) is a metal-rich clast consisting of enstatite and a silica mineral set in metal.
Some enstatite grains include an aggregate of tiny metal and pyroxene, with a composition
of ferroan orthopyroxene (En_{83}). Plagioclase grains are very rare. Width, about 440 μ.

(d) Clast δ4 (E2) is a metal-rich clast consisting of enstatite and metal-sulfide network. The
enstatite contains tiny metal grains in it. Width, about 260 μ.

olivine ($Fo_{>95}$) which may have been produced by reduction from more ferroan
olivine (Figs. 2i, j), because the forsterites contain tiny metal grains in their cores.
Pyroxenes in this type are minor (Fig. 2j) and are diopside, rarely orthopyroxene.

Granular Ol-rich clasts (B4) have euhedral olivine with Fo_{74-84}, with minor
low-Ca pyroxene and alkali-free glass (Figs. 2k, l). Magnesian orthopyroxene or
pigeonite grains occur in alkali-free glass in this type, and they may have crystallized
from a melt under rapid cooling conditions. The interstitial glasses are extremely
depleted in Al_2O_3 and alkali components (Table 3a), and may correspond to low-Ca
pyroxenes in composition. This type may be shocked, reduced and/or melted lithic
fragments.

4.3. Felsic lithic clasts (C)

The predominant clast types in this group are porphyritic igneous rocks (C1;
Figs. 3a–f) and pilotaxitic plagioclase (Pl)-rich rocks (C2; Figs. 3g, h). Rare clast
types include glassy (C3; Figs. 3i, j) and gabbroic (C4; Fig. 3k, l) clasts, including
troctolitic and calcic Pl-Aug assemblages. Representative chemical compositions of

Fig. 6. Back scattered electron images of chondrules and chondritic fragments. Symbols in parentheses after clast numbers correspond to groups in Table 1.

(a) Clast α14 (F1-1) is a fragment of a barred olivine chondrule, consisting of barred olivine (Fo$_{71-72}$) and a groundmass with a minor amount of orthopyroxene. Width, about 800 μ.

(b) Clast α41 (F1-2) is a porphyritic olivine chondrule. The olivine shows normal zoning from Fo$_{97-72}$. The groundmass consists of glass and needle-like pyroxene. Width, about 800 μ.

(c) Clast α33B (F1-3) is a porphyritic olivine-pyroxene chondrule. Width, about 700 μ.

(d) Clast α36C (F1-4) is a porphyritic enstatite-diopside chondrule, with interstitial glass. Width, about 400 μ.

(e) Clast δ7 (F1-5) is a radial pyroxene chondrule consisting mainly of enstatite, interstitial glass, and tiny sulfides. Width, about 1 mm.

(f) Clast α43 (F2) is a fragment of a chondrite, consisting mainly of olivine (Fo$_{78-66}$), orthopyroxene, and plagioclase (An$_{6-11}$). Width, about 800 μ.

the minerals in these clasts are given in Tables 4a, b.

The porphyritic type (C1) consists of pyroxene and plagioclase phenocrysts and fine-grained dacitic groundmass (Figs. 3a, b, e). Pyroxene phenocrysts sometimes have ferroan cores and magnesian mantles (Fig. 3c), suggesting that reduction took place during their crystallization. The groundmass pyroxenes are often more
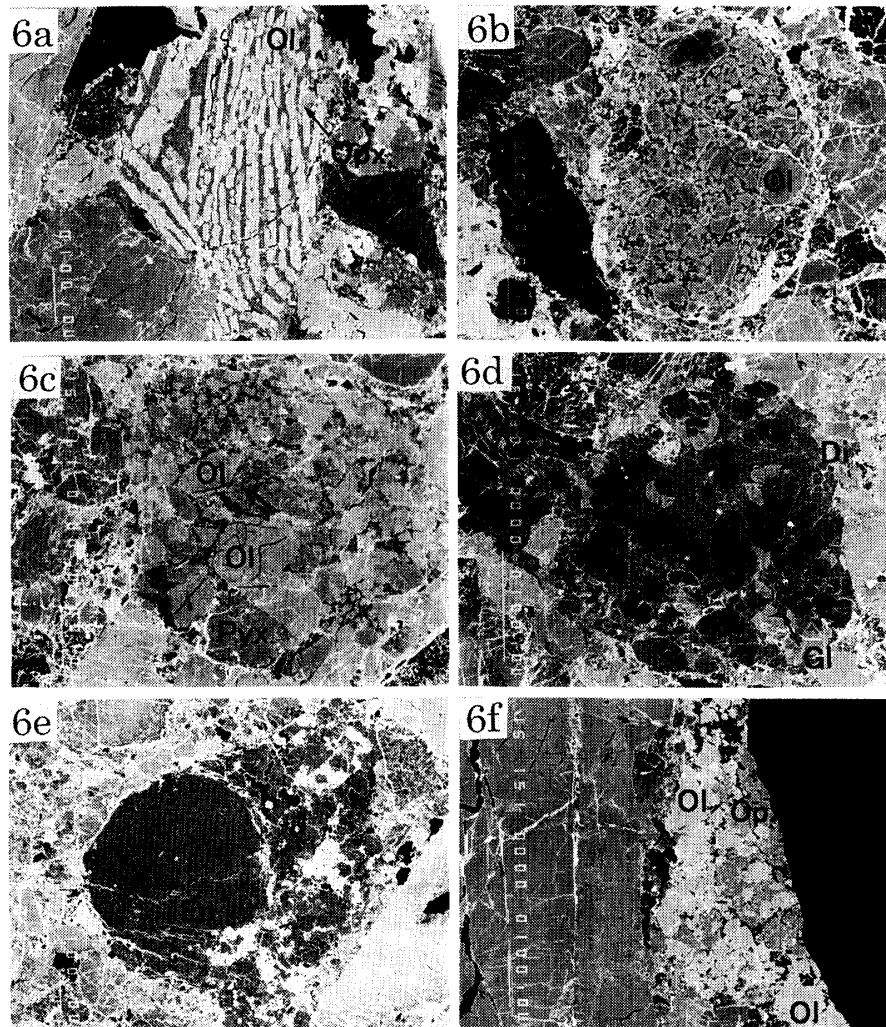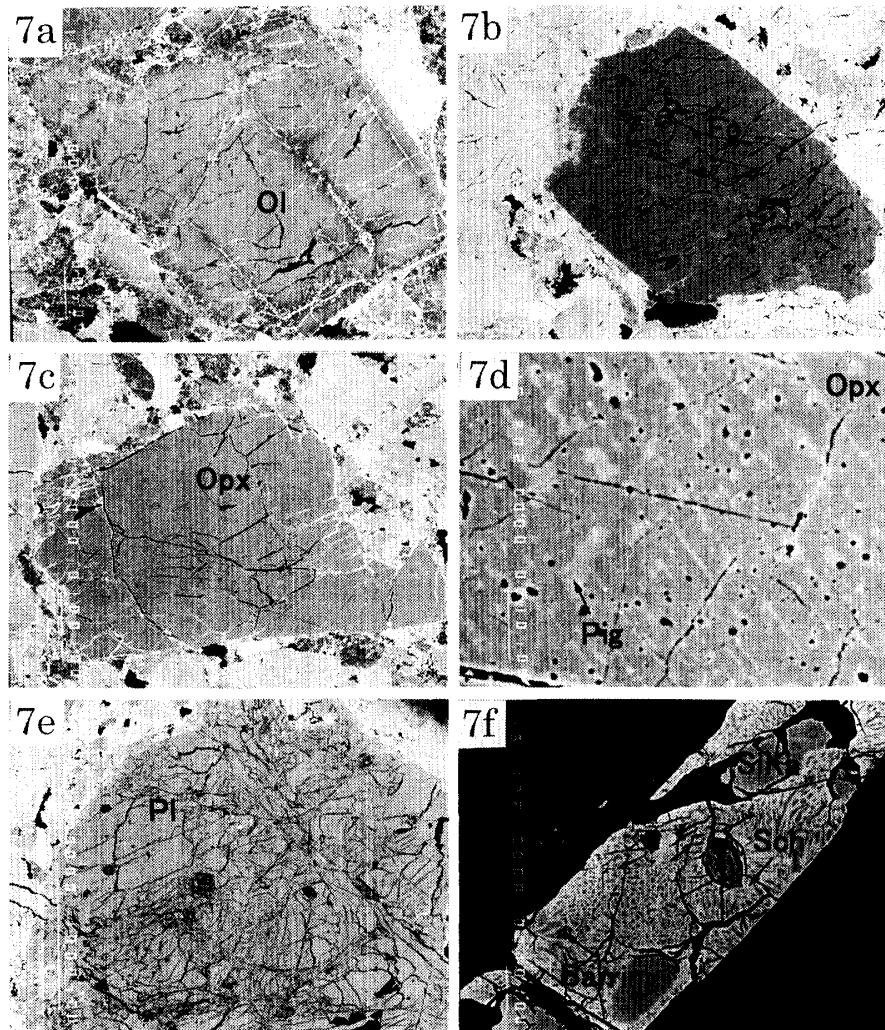
Fig. 7.   Back scattered electron images of isolated mineral clasts.   Symbols in parentheses after
          clast numbers correspond to groups in Table 1.
(a)   Clast α18B (G1-1) is an isolated olivine grain (Fo$_{82-84}$).   Width, about 860 μ.
(b)   Clast α18A (G1-3) is an isolated magnesian olivine grain (Fo$_{100}$).   Width, about 1.2 mm.
(c)   Clast α20A (G2-1) is an isolated orthopyroxene grain (En$_{88}$Fs$_8$Wo$_4$).   Width, about 630 μ.
(d)   Clast α8E (G2-3) is an isolated pyroxene grain, consisting of orthopyroxene host and
      pigeonite lamellae.   Width, about 60 μ.
(e)   Clast α22 (G3-2) is a large isolated plagioclase grain.   Width, about 3 mm.
(f)   Clast α5E (G8-2) is an isolated metal grain, consisting of schreibersite and barringerite with
      nodules of Si-bearing kamacite.   Width, about 100 μ.

ferroan (mg < 0.50) than the cores and mantles of the phenocrysts (Table 4a), and
they probably crystallized in a closed system under rapid cooling conditions.
Plagioclase in this type occurs as phenocrysts and groundmass minerals. Sometimes
the plagioclase phenocrysts show reverse zoning, with sodic cores and calcic mantles
(Fig. 3d). This reverse zoning may have happened at the same time as the reverse
zoning of the pyroxene phenocrysts (Fig. 3c). Clasts of this type include glasses in
their groundmass and are rich in sodic plagioclase and orthoclase components, as
well as SiO$_2$. The TiO$_2$ content of the glasses is high (> 1 wt%), and their mg ratios

Y. Ikeda, M. Prinz and C. E. Nehru

Table 3a.   Chemical compositions of silicate minerals and glasses in fine-grained mafic lithic clasts (group B).

Type	B1	B1	B1	B1	B1	B1	B1	B1	B1	B1	B1	B1	B1	B1	B1	B1	B1	B1
Clast	α6	α6	α6	α6	α6	α35B	α35B	α35B	α35B	α35B	α35B	α35B	δ1	δ1	δ1	δ1	δ1	δ1
No.	117	1367	111	541	1368	1061	1063	1110	1113	1059	1065	1111	32	40	113	114	52	119
Mineral	Ol	Ol	Opx	Opx	Aug	Ol	Ol	Opx	Opx	Aug	Aug	Silica	Ol-core	Ol-rim	Pig	Opx	Aug	Pl
SiO2	41.30	39.91	56.92	56.70	54.19	41.61	41.98	56.32	58.98	56.23	56.16	97.68	38.25	42.33	56.49	58.12	55.19	66.36
TiO2	0.00	0.00	0.00	0.00	0.11	0.00	0.00	0.01	0.01	0.04	0.00	0.00	0.00	0.00	0.01	0.00	0.18	0.13
Al2O3	0.01	0.02	0.02	0.09	0.57	0.00	0.00	0.00	0.16	2.82	0.13	0.17	0.00	0.00	0.57	0.29	1.66	20.43
Cr2O3	0.65	0.85	1.09	1.06	1.22	0.93	0.82	0.72	0.18	0.83	1.04	0.00	0.50	0.64	1.05	0.68	0.57	0.00
FeO	0.70	8.02	5.00	4.87	5.01	4.95	4.30	6.40	0.32	3.02	3.64	0.30	20.67	1.28	11.18	8.21	0.75	0.54
MnO	0.48	0.67	0.48	0.22	0.46	0.67	0.57	0.18	0.07	0.60	0.46	0.00	0.52	0.65	0.37	0.38	0.31	0.18
MgO	56.47	49.62	35.11	32.30	21.61	51.10	50.99	34.25	37.16	22.28	25.60	0.24	39.83	53.60	25.91	32.49	22.75	0.00
CaO	0.37	0.34	1.22	3.06	16.90	0.25	0.40	0.45	2.57	12.83	12.15	0.07	0.22	0.45	4.54	0.38	17.27	2.29
Na2O	0.00	0.04	0.00	0.05	0.14	0.00	0.00	0.03	0.00	0.44	0.07	0.02	0.04	0.01	0.03	0.03	0.10	10.39
K2O	0.01	0.00	0.00	0.00	0.00	0.00	0.00	0.01	0.00	0.00	0.00	0.00	0.02	0.00	0.00	0.00	0.00	0.47
Total	99.99	99.47	99.84	98.35	100.15	99.51	99.07	98.36	99.45	99.09	99.25	98.50	100.03	98.96	100.15	100.58	98.78	100.79
mg ratios	0.99	0.92	0.93	0.92	0.88	0.95	0.95	0.91	1.00	0.93	0.93		0.77	0.99	0.81	0.88	0.98	

Type	B2	B2	B2	B2	B2	B2	B2	B2	B2	B2	B2	B2	B2	B2	B2	B2	B2	B2
Clast	α7C	α7C	α7C	α7C	α7C	α33A	α33A	α33A	α33A	α33A	α33A	α33A	α37C	α37C	α37C	α37C	α30A	α30A
No.	709	721	717	718	719	674	675	1892	1890	1895	1889	1894	691	1178	692	1177	2024	2025
Mineral	Pig	Pig	Opx	Aug	Gl	Pig	Opx	Opx	Aug	Pl	Gl	Silica	Pig	Pig	Opx	Opx	En	En
SiO2	55.15	55.65	54.80	52.28	68.12	54.89	55.77	56.00	55.64	62.28	66.58	95.17	54.99	54.76	55.92	55.73	60.01	60.23
TiO2	0.02	0.00	0.07	0.10	0.16	0.00	0.00	0.00	0.43	0.00	0.04	0.09	0.00	0.03	0.00	0.00	0.08	0.00
Al2O3	0.18	0.30	0.22	0.75	16.35	1.07	0.14	0.17	0.83	22.10	19.15	2.17	1.19	1.09	0.16	0.19	0.06	0.22
Cr2O3	0.99	0.90	1.09	1.11	0.00	1.17	1.06	1.21	0.27	0.00	0.09	0.04	1.21	1.31	1.26	1.27	0.07	0.00
FeO	5.47	4.93	6.09	2.93	0.41	11.45	9.31	9.14	0.35	0.52	0.92	0.50	11.62	11.83	10.07	8.53	0.38	0.54
MnO	0.70	0.75	0.65	0.59	0.17	0.39	0.41	0.37	0.23	0.00	0.00	0.00	0.31	0.09	0.29	0.20	0.39	0.00
MgO	31.16	31.23	31.52	24.06	2.40	25.32	28.73	29.59	22.41	0.32	1.56	0.16	24.98	24.50	28.01	29.12	39.84	38.87
CaO	5.02	4.91	3.77	17.25	5.04	5.62	2.80	2.00	17.83	11.92	6.54	0.85	5.59	5.69	3.31	3.52	0.17	0.33
Na2O	0.14	0.07	0.01	0.08	3.61	0.15	0.02	0.00	0.03	1.17	4.23	0.35	0.05	0.07	0.00	0.02	0.00	0.00
K2O	0.00	0.00	0.00	0.00	0.17	0.00	0.00	0.00	0.00	0.00	0.00	0.00	0.00	0.00	0.03	0.00	0.00	0.00
Total	98.83	98.74	98.22	99.15	96.43	100.06	98.24	98.48	98.02	98.31	99.11	99.33	99.94	99.40	99.02	98.61	101.00	100.19
mg ratios	0.91	0.92	0.90	0.94	0.91	0.80	0.85	0.85	0.99		0.75		0.79	0.79	0.83	0.86	0.99	0.99

Type	B3	B3	B3	B3	B4	B4	B4	B4	B4	B4	B4	B4	B4
Clast	α32B	α32B	α32B	α32B	α8B	α8B	α8B	α8B	α8B	α16B	α16B	α16B	α16B
No.	1878	1880	1882	1885	557	612	558	602	604	644	648	647	645
Mineral	Ol	Ol	En	Aug	Ol	Ol	Pig	Gl	Gl	Ol	Ol	Gl	Gl
SiO2	43.09	43.27	58.33	57.69	39.11	39.01	53.00	54.16	55.51	39.12	39.02	56.82	56.89
TiO2	0.01	0.02	0.09	0.03	0.00	0.00	0.07	0.00	0.00	0.00	0.00	0.00	0.00
Al2O3	0.05	0.02	1.91	0.58	0.00	0.04	0.68	0.83	0.65	0.00	0.00	0.08	0.07
Cr2O3	0.35	0.00	0.00	0.96	0.64	0.62	1.78	1.58	1.42	0.60	1.03	1.13	1.02
FeO	0.60	0.44	0.30	1.70	20.19	19.82	14.84	15.83	15.40	18.67	18.58	10.52	10.57
MnO	0.36	0.14	0.17	0.42	0.35	0.32	0.10	0.49	0.33	0.42	0.13	0.25	0.33
MgO	55.83	56.29	36.55	24.82	39.69	40.37	24.19	22.63	23.58	40.65	40.15	30.28	30.30
CaO	0.24	0.25	2.75	15.22	0.26	0.30	3.67	4.50	3.98	0.39	0.26	0.93	0.61
Na2O	0.00	0.00	0.00	0.00	0.07	0.00	0.01	0.04	0.00	0.02	0.02	0.02	0.03
K2O	0.03	0.00	0.00	0.00	0.00	0.00	0.00	0.00	0.00	0.00	0.00	0.00	0.00
Total	100.56	100.43	100.10	101.42	100.31	100.48	98.34	100.06	100.87	99.87	99.19	100.03	99.82
mg ratios	0.99	1.00	1.00	0.96	0.78	0.78	0.74	0.72	0.73	0.80	0.79	0.84	0.84

Table 3b.   Chemical compositions of metal and sulfide in fine-grained mafic lithic clasts (group B).

Type	B1	B1	B1	B1	B1	B1	B1	B1	B1	B2	B2	B2	B3
Clast	$\alpha 6$	$\alpha 6$	$\alpha 6$	$\alpha 6$	$\alpha 35B$	$\alpha 35B$	$\delta 1$	$\delta 1$	$\delta 1$	$\alpha 30A$	$\alpha 30A$	$\alpha 30A$	$\alpha 32B$
No.	M23	M24	M31	M36	M142	M144	M2	M31	M87	M137	M135	M157	M141
Mineral	Ka	Sues	Sues	Sulfide	Sues	Ka	Ka	Ka	alt.Daub	Tae	Sulfide	Daub	Ka
Si	7.90	15.65	15.89	0.05	15.96	12.46	5.90	5.52	0.00	0.35	0.02	0.00	6.5
P	0.24	0.01	0.04	0.01	0.01	0.09	0.48	0.21	0.01	0.07	0.00	0.00	0.11
S	0.00	0.00	0.00	36.72	0.01	0.00	0.00	0.02	41.76	0.03	37.04	42.22	0.01
Cr					0.60	1.99			30.45	0.02	1.20	35.95	2.08
Mn					0.04	0.00			0.56	0.00	0.00	2.83	0
Fe	89.14	81.67	81.91	61.37	82.47	84.23	89.86	89.78	21.20	81.08	59.73	16.04	88.02
Co	0.28	0.28	0.21	0.18	0.16	0.21	0.33	0.37	0.00	0.32	0.09	0.05	0.18
Ni	1.16	1.34	1.32	0.84	0.92	0.69	2.82	4.21	0.03	17.48	0.02	0.04	0.18
Total	98.72	98.95	99.37	99.17	100.17	99.67	99.39	100.11	94.01	99.35	98.10	97.13	97.08

are less than 0.20 (Table 4a).

A porphyritic felsic clast (C1, $\alpha 34$), about 1.5 mm × 1 mm, contains several phenocrysts of plagioclase and pyroxene (Figs. 3b, c, d). Pyroxene phenocrysts have reverse zoning; the core is ferroan pigeonite, $En_{51-53}Wo_{10}$, and the mantle is more magnesian augite with $En_{48}Wo_{37}$. Plagioclase phenocrysts, about 0.3 mm across, have reverse zoning; the cores are sodic (An_{7-9}) and the mantles are more calcic to sodic (Table 4a), where the inner mantles are more calcic (An_{15-21}) and the outer mantles are more sodic (An_{4-10}). A whitlockite grain, 40 × 80 microns, occurs as a microphenocryst (Fig. 3c). The groundmass consists mainly of sodic plagioclase (An_{2-9}), ferroan pyroxene, and minor rhyolitic glass.

A porphyritic felsic clast (C1, $\gamma 15$) is large, 2 mm × 1.5 mm across, and consists mainly of plagioclase, pigeonite, and augite phenocrysts and minor dacitic groundmass (Figs. 3e, f). The plagioclase phenocrysts have normal zoning (An_{3-10}) and include small grains of pigeonite. The groundmass consists of rhyolitic glass with tiny needle-like augites. Microphenocrystic ilmenite occurs in contact with the groundmass or as inclusions in pigeonite phenocrysts. Whitlockite grains are found as tiny inclusions in plagioclase phenocrysts, and apatite occurs as microphenocrysts in contact with the groundmass.

Pilotaxitic type clasts (C2) consist mainly of plagioclase laths with minor amounts of pyroxene. The plagioclase laths have cores of An_{40-55} with sodic rims of An_{30-40}. Pyroxenes occur as small grains in interstitial spaces between plagioclase laths (Figs. 3g, h). They are always magnesian (mg > 0.90) and sometimes have slight normal zoning from magnesian low-Ca pyroxene cores to less-magnesian high-Ca pyroxene rims. The mesostasis in this type seems to be a mixture of feldspar and silica, although the silica mineral is too small to analyze.

A pilotaxitic clast (C2; $\alpha 24B$), 0.3 mm × 1 mm, consists of small laths of plagioclase, 10–20 microns long and 2–10 microns wide, with interstitial pyroxene and sodic mesostasis (Figs. 3g, h). The plagioclase laths are An_{30-55}, but the mesostasis is more sodic (An_{2-10}) in normative composition and seems to contain silica. The interstitial pyroxene is mainly augite ($En_{54-67}Wo_{28-43}$), with pigeonitic cores ($En_{82-86}Wo_{7-10}$).

A magnesian glassy clast (C3-1; $\alpha 8$), 500 × 800 microns, consists mainly of glass with microphenocrysts of enstatite, quenched needles of diopside, and minor spherules of sulfide (Fig. 3i). The microphenocrystic enstatite and the needle-like diopside are almost FeO-free (Table 4a). The sulfide spherules, about 10 microns

Y. Ikeda, M. Prinz and C. E. Nehru

Table 4a. Chemical compositions of silicate and oxide minerals and glasses in felsic clasts (group C).

Type	C1	C1	C1	C1	C1	C1	C1	C1	C1	C1	C1	C1	C1	C1	C1
Clast	α 13A	α 13A	α 13A	α 13A	α 19A	α 19A	α 19A	α 19A	α 34	α 34	α 34	α 34	α 34	α 34	α 34
No.	138	135	1486	1471	810	203	1037	803	1847	1853	1869	1874	1008	22	1002
Mineral	Pl	Aug	Gdm-Pig	Chm	Pl	Aug	Ulvosp	Gl	Pl-core	Pl-rim	Pyx-core	Pyx-rim	Gdm-Pl	Gdm-Pig	Gl
SiO2	62.91	53.00	50.85	0.17	66.34	53.32	0.55	72.82	66.38	63.40	51.93	53.16	67.09	49.55	71.33
TiO2	0.09	0.61	0.39	4.46	0.10	0.54	34.11	2.00	0.00	0.00	0.69	0.68	0.12	0.74	1.22
Al2O3	22.96	0.92	1.17	7.32	20.25	0.79	0.11	7.59	20.07	22.43	0.22	0.88	20.06	0.16	9.90
Cr2O3	0.00	1.02	0.16	50.87	0.00	1.23	0.16	0.00	0.00	0.00	0.33	1.09	0.00	0.09	0.00
FeO	0.43	9.73	25.09	26.54	0.26	8.64	60.81	7.71	0.34	0.22	23.30	10.83	0.43	33.34	8.39
MnO	0.09	0.55	1.20	0.98	0.06	0.50	1.27	0.19	0.00	0.00	1.18	1.13	0.05	1.56	0.00
MgO	0.06	15.64	13.95	7.28	0.05	16.41	0.16	0.25	0.01	0.04	17.15	17.16	0.01	10.90	0.14
CaO	4.70	17.76	6.22	0.25	2.07	17.45	0.00	0.25	1.72	4.38	4.62	15.00	1.03	3.40	0.17
Na2O	9.15	0.48	0.59	0.05	10.44	0.66	0.00	2.70	10.54	8.74	0.17	0.46	10.79	0.20	3.54
K2O	0.11	0.02	0.02	0.00	0.28	0.00	0.00	2.98	0.38	0.29	0.00	0.00	0.78	0.00	2.87
Total	100.50	99.73	99.64	97.92	99.85	99.54	97.17	96.49	99.44	99.50	99.59	100.39	100.36	99.94	97.56
mg ratios		0.74	0.50	0.33		0.77	0.00	0.05			0.57	0.74		0.37	0.03

Type	C1	C1	C1	C1	C1	C1	C1	C1	C1	C1	C2	C2	C2	C2	C3-1	C3-1	C3-1	C3-1
Clast	δ 15	δ 15	δ 15	δ 15	δ 15	δ 13A	δ 13A	δ 13A	δ 13A	δ 13A	α 24B	α 24B	α 24B	α 24B	α 8A	α 8A	α 8A	α 8A
No.	79	69	70	61	434	225	239	243	247	257	83	868	864	871	42	51	1557	1561
Mineral	Pl	Pig	Aug	Ilm	Gl	Pl	Gdm-Pl	Gdm-Aug	Gdm-Opx	Gl	Pl	Gdm-Pl	Gdm-Aug	Meso	En	Aug	Gl	Gl
SiO2	65.96	51.30	52.05	0.07	70.36	64.59	68.11	52.31	49.02	71.06	56.02	65.97	54.35	70.82	59.93	56.64	71.87	70.07
TiO2	0.19	0.48	1.22	53.86	1.41	0.00	0.15	1.05	0.64	1.22	0.00	0.00	0.03	0.03	0.17	0.48	0.07	0.08
Al2O3	20.33	0.15	0.30	0.03	12.52	21.33	19.03	1.62	0.33	8.62	26.71	20.23	1.84	17.43	0.36	1.86	14.50	13.60
Cr2O3	0.00	0.27	0.87	1.81	0.08	0.00	0.00	1.51	0.02	0.00	0.00	0.00	1.66	0.00	0.03	0.00	0.14	0.00
FeO	0.08	27.23	13.95	38.99	3.92	0.43	0.66	10.73	34.97	9.01	0.27	0.36	2.91	0.32	0.45	0.20	0.14	0.14
MnO	0.00	1.54	0.54	0.89	0.00	0.08	0.00	1.14	1.85	0.28	0.07	0.00	0.29	0.00	0.29	0.00	0.00	0.00
MgO	0.00	15.31	12.32	3.44	0.55	0.05	0.02	16.11	10.43	0.21	0.08	0.52	19.08	0.09	39.03	22.61	1.99	3.07
CaO	1.85	4.03	16.96	0.00	0.31	3.19	0.73	15.39	2.91	0.13	10.20	1.94	19.56	0.41	0.47	17.71	2.93	3.79
Na2O	10.54	0.25	0.66	0.06	8.75	9.75	11.13	0.72	0.15	3.23	5.97	10.54	0.57	10.94	0.04	0.59	7.57	7.41
K2O	0.59	0.00	0.01	0.02	1.27	0.20	0.51	0.00	0.00	3.78	0.00	0.08	0.00	0.11	0.00	0.06	0.73	0.74
Total	99.54	100.56	98.88	99.17	99.17	99.62	100.34	100.58	100.32	97.54	99.32	99.64	100.29	100.15	100.77	100.15	99.94	98.90
mg ratios		0.50	0.61	0.14	0.20			0.73	0.35	0.04			0.92	0.33	0.99	1.00	0.96	0.98

Type	C3-2	C3-2	C3-2	C3-2	C3-2	C3-2	C4-1	C4-1	C4-2	C4-2
Clast	α 16A	α 16A	α 16A	α 16A	α 16A	α 16A	δ 8	δ 8	α 21B	α 21B
No.	176	178	180	181	185	1572	201	211	838	839
Mineral	Ol-core	Ol-rim	Pyx-core	Pyx-rim	Gdm-Aug	Gl	Pl	Ol	Aug	Pl
SiO2	39.57	38.50	54.72	50.00	51.39	62.32	46.30	41.26	49.12	43.19
TiO2	0.00	0.00	0.00	0.08	0.51	0.60	0.00	0.00	0.69	0.00
Al2O3	0.00	0.00	0.71	1.56	5.09	12.40	33.86	0.05	4.89	35.36
Cr2O3	0.55	0.65	1.50	2.25	2.19	0.26	0.00	0.24	0.81	0.00
FeO	13.75	17.27	12.91	23.18	18.09	12.93	0.31	6.35	9.72	0.31
MnO	0.32	0.23	0.42	0.71	0.63	0.11	0.00	0.15	0.26	0.00
MgO	46.10	42.79	28.31	17.79	7.99	0.75	0.23	50.76	11.63	0.06
CaO	0.05	0.12	0.64	3.13	12.70	8.08	17.15	0.19	23.09	19.81
Na2O	0.02	0.04	0.01	0.00	0.30	1.15	1.41	0.07	0.05	0.09
K2O	0.00	0.00	0.00	0.09	0.16	0.16	0.00	0.02	0.00	0.00
Total	100.36	99.60	99.22	98.70	98.98	98.76	99.26	99.09	100.26	98.82
mg ratios	0.86	0.82	0.80	0.58	0.44	0.09		0.93	0.68	

Gdm: groundmass

Table 4b. Chemical compositions of metal in felsic clasts (group C).

Type	C2
Clast	α 24B
No.	M126
Mineral	Ta
Si	0.07
P	0.00
S	0.14
Fe	85.71
Co	0.28
Ni	12.28
Total	98.48

across, occur in the glass and are rich in Cr, Mn, and Mg. The glass has a rhyolitic composition (Table 4a), but is extremely magnesian with mg$=0.98$ and poor in TiO_2 (<0.1 wt%; Table 4a). The normative feldspar composition of the glass is An_8.

A ferroan glassy clast (C3-2; α16A), $100\,\mu \times 200\,\mu$, consists of olivine and low-Ca pyroxene phenocrysts and ferroan CaO-rich glassy groundmass (Fig. 3j). The olivine phenocrysts have normal zoning, from Fo_{86} to $Fo_{<82}$, and the low-Ca pyroxene phenocrysts have orthopyroxene cores with mg$=0.80$–0.60 and pigeonitic rims with mg <0.60, showing normal zoning. The glassy groundmass includes feather-like augite set in glass. The glass is ferroan (mg$=0.09$) and rich in CaO (Table 4a), and the SiO_2 content is moderate ($SiO_2 = 62$ wt%).

The troctolitic assemblage (C4.1; Fig. 3k) consists of coarse-grained plagioclase (An_{87}) and olivine (Fo_{93}), and may be a plutonic rock type. Plagioclase-fassaitic pyroxene clasts, which were thought to relate with Angra Dos Reis, occur in Nilpena and North Haig (Prinz *et al.*, 1986), and a small clast similar to the ADOR-like clasts is found in DAG 319. It consists of fassaitic augite with 5 wt% of Al_2O_3 and calcic plagioclase (An_{99}) (C4.2; Fig. 3l). It may be a fragment of one of the gabbroic lithologies and its genetic relationship with the angrites is uncertain.

4.4. Dark clasts (D)

Numerous dark lithic clasts (Figs. 4a–l), up to several mm across, are present. They consist mainly of phyllosilicate phases, but also contain olivine, sulfides, magnetite (sometimes as framboids which are aggregates of tiny spherules), and/or Ca-Fe-Mg carbonates. These are very similar to the dark inclusions found in Nilpena and North Haig, described in Brearley and Prinz (1992). There are two types of dark clasts: (D1) fayalite (Fa)-free clasts, which are common, and (D2) Fa-bearing clasts, which are rare. Representative chemical compositions of the minerals in these clasts are shown in Tables 5a, b.

In the Fa-free dark clasts (D1), phyllosilicates are predominant, and sulfide, magnetite, and carbonates are minor. Phyllosilicates occur as matrix minerals (Figs. 4a–l), isolated fragments or nodules (Fig. 4f, g), and vein minerals (Figs. 4b, c, d). Sulfides are mainly pyrrhotite and have their euhedral outlines. Carbonates are dolomite or magnesite, and sometimes occur as fragments of large carbonate grains (Fig. 4f). Calcite veins penetrate different types of clasts, suggesting they are terrestrial alteration products. Phosphates occur as tiny grains set in the hydrated matrix and never occur as large crystals. Magnesian olivines and pyroxenes occur as exotic isolated fragments set in the hydrated matrix, but fayalitic olivines do not occur in this clast type.

A Fa-free dark clast (D1; α25A), 1 mm$\times$0.7 mm, consists mainly of dark phyllosilicate matrix with variable amounts of sulfide and magnetite (Fig. 4a). The matrix contains tiny phosphate grains and probable carbonaceous materials. A phyllosilicate vein (Fig. 4b) occurs in the clast and includes dolomite which is sometimes surrounded by phyllosilicates. The phyllosilicate vein stops at the boundary of the clast, indicating it is endogenetic. However, there are narrow

Table 5a. Chemical compositions of silicate and oxide minerals in dark clasts (group D).

Type	D1	D1	D1	D1	D1	D1	D1	D1	D1	D1	D1	D1	D1	D1	D1	D1
Clast	α7B	α7B	α7B	α7B	α7B	α7B	α25A	α25A	α25A	α28B	α28B	α28B	γ3	γ3	γ3	γ3
No.	760	749	1015	549	1457	750	901	876	1045	967	965	664	168	121	152	164
Mineral	Phyllosil	Phyllosil	Dolomite	Dolomite	Mt	Mt	Vein-phyll	Vein-phyll	Dolomite	Matrix	Matrix	Mt	Nodule-ph	Matrix	Dolomite	Mt
SiO2	37.17	36.19	0.35	0.17	0.07	0.04	34.56	38.25	0.61	34.34	32.14	0.00	39.40	38.39	0.10	0.00
TiO2	0.06	0.01	0.04	0.09	0.00	0.00	0.00	0.00	0.07	0.04	0.00	0.00	0.05	0.00	0.05	0.00
Al2O3	1.29	1.15	0.00	0.00	0.02	0.02	5.75	4.74	0.00	1.94	1.79	0.05	2.36	2.65	0.00	0.00
Cr2O3	0.49	0.38	0.06	0.10	0.00	0.00	0.10	0.08	0.12	0.31	0.41	0.00	0.75	0.63	0.08	0.00
FeO	20.52	19.67	5.32	5.26	89.82	90.91	25.93	23.33	8.38	24.38	27.08	90.66	9.62	16.13	6.09	92.22
MnO	0.15	0.05	3.61	1.40	0.21	0.00	0.11	0.19	1.96	0.00	0.00	0.00	1.25	0.44	3.06	0.00
MgO	24.16	24.89	13.85	17.22	0.17	0.05	20.89	18.14	34.07	18.36	17.78	0.00	29.59	27.00	15.83	0.00
CaO	0.67	0.23	29.35	28.26	0.00	0.21	0.23	1.66	7.19	1.68	1.18	0.16	0.09	0.05	26.33	0.00
Na2O	0.01	0.02	0.06	0.03	0.04	0.07	0.10	0.75	0.02	0.46	0.07	0.00	0.00	0.04	0.00	0.00
K2O	0.00	0.00	0.03	0.00	0.00	0.01	0.44	0.40	0.01	0.30	0.20	0.00	0.06	0.13	0.00	0.00
Total	84.52	82.59	52.67	52.53	90.33	91.31	88.11	87.54	52.43	81.81	80.65	90.87	83.17	85.46	51.54	92.22
mg ratios	0.68	0.69	0.82	0.85	0.00	0.00	0.59	0.58	0.88	0.57	0.54	0.00	0.85	0.75	0.82	0.00

Type	D1	D1	D1	D1	D1	D1	D1	D1	D2	D2	D2	D2	D2	D2	D2
Clast	δ5	δ5	δ5	δ5	δ5	δ6	δ6	δ6	α27A	α27A	α27A	α27A	α27A	α27A	α27A
No.	91	180	100	176	158	340	313	320	1959	1939	936	937	1514	1516	2009
Mineral	Nodule-ph	Nodule-ph	Vein-ph	Vein-ph	Matrix	Nodule-ph	Phyllo sili	Mt	Matrix	Matrix	Mt	Fa-core	Fa-rim	Fa-rim	Ol
SiO2	45.59	40.76	38.60	41.15	33.65	38.70	40.02	0.75	43.62	37.42	0.00	29.57	29.68	30.91	42.09
TiO2	0.02	0.00	0.00	0.03	0.00	0.00	0.00	0.05	0.02	0.05	0.00	0.00	0.00	0.00	0.18
Al2O3	1.12	1.86	2.13	4.98	3.56	1.97	3.51	0.00	4.15	4.98	0.00	0.00	0.08	0.46	0.05
Cr2O3	0.66	0.78	0.99	0.23	3.77	0.04	0.44	0.00	0.31	0.21	0.00	0.00	0.00	0.00	0.3
FeO	13.96	11.08	12.96	14.66	19.07	24.57	14.05	91.33	12.33	20.91	90.45	68.76	66.37	55.21	1.36
MnO	0.10	0.18	0.22	0.13	0.14	0.45	0.15	0.06	0.14	0.00	0.00	0.46	1.02	0.51	0.39
MgO	24.14	33.11	30.16	24.14	24.72	24.30	30.12	0.04	24.64	20.37	0.40	0.55	2.18	11.02	55.16
CaO	0.79	0.67	1.03	1.47	0.24	1.90	0.42	0.00	0.51	0.67	0.02	0.03	0.13	0.07	0.16
Na2O	0.82	0.69	0.84	0.41	0.29	0.75	0.65	0.04	0.64	1.22	0.08	0.10	0.05	0.20	0.03
K2O	0.21	0.09	0.03	0.15	0.00	0.07	0.14	0.00	0.45	0.62	0.00	0.00	0.00	0.08	0
Total	87.41	89.22	86.96	87.35	85.44	92.75	89.50	92.27	86.81	86.45	90.95	99.47	99.51	98.46	99.72
mg ratios	0.76	0.84	0.81	0.75	0.70	0.64	0.79	0.00	0.78	0.63	0.01	0.01	0.06	0.26	0.99

Table 5b. Chemical compositions of metal and sulfide in dark clasts (group D).

Type	D1	D1	D1	D1	D1	D1	D2
Clast	α7B	α7B	α28B	γ3	δ5	δ5	α27A
No.	M45	M47	M104	M99	M45	M44	M101
Mineral	Pyrrh	Pent	Pyrrh	Pyrrh	Pyrrh	Pent	Pyrrh
Si	0.04	0.09	0.06	0.01	0.01	0.02	0.04
P	0.01	0.00	0.00	0.00	0.01	0.02	0.00
S	39.59	35.66	39.93	37.83	38.83	39.03	38.38
Cr			0.03	0.00			0.02
Mn			0.00	0.00			0.00
Fe	59.08	29.49	54.91	59.04	59.01	53.75	59.00
Co	0.04	1.57	0.23	0.11	0.13	0.47	0.11
Ni	0.78	33.11	3.48	0.85	0.75	4.23	0.24
Total	99.54	99.92	98.64	97.84	98.74	97.52	97.79

calcite veins (Fig. 4b) which continue outside the clast, suggesting they were produced by terrestrial weathering processes. Another large dark clast (D1; δ5), 4 mm $\times$ 2 mm, contains phyllosilicate veins (Fig. 4c), and a broad phyllosilicate vein cut by a narrow phyllosilicate vein (Fig. 4d). Two fayalite-free dark clasts, 700 $\mu \times 350 \mu$ (D1; α7B), and 3 mm $\times$ 2 mm (D1; γ3), have dolomite fragments, phyllosilicate aggregates, rounded magnetites and lath-shaped sulfides, all set in a phyllosilicate matrix (Fig. 4f). They often include exotic anhydrous lithic clasts such as magnesian olivine, pigeonite, and rhyolitic glass (Fig. 4e). These exotic clasts are unaltered, even when in direct contact with the phyllosilicate matrix. Another dark clast (D1; δ6), 2 mm $\times$ 0.5 mm, contains phyllosilicate fragments and magnetite framboids set in the matrix (Figs. 4g, h).

Fa-bearing dark clasts (D2) contain ferroan olivines in the hydrated matrix. In a fayalite-bearing clast (D2; α27), 1 mm $\times$ 0.7 mm, fayalite grains occur directly in the phyllosilicate matrix (Fig. 4l) and have reverse zoning from Fo_1 to Fo_{26}. Magnetite also occurs as rounded or subrounded grains in the matrix of this clast (Fig. 4j) and at the peripheral portions of sulfides (Fig. 4k). A few large igneous lithic fragments are included, consisting of olivine and/or orthopyroxene phenocrysts and groundmass (Fig. 4i); a basaltic lithic fragment consists mainly of olivine phenocrysts and groundmass, the olivine phenocrysts show normal zoning from Fo_{99} to $Fo_{<75}$, and small grains of ferroan olivines occur in the groundmass. The groundmasses of the igneous fragments experienced hydrous alteration, suggesting that the hydration and formation of fayalite took place *in situ* in the Fa-bearing clasts. Magnesian olivine, which is a constituent mineral of the lithic igneous fragments, occurs directly in the matrix as isolated grains (Fig. 4j). Therefore, olivines in this clast type are bimodal in composition, with magnesian ($Fo_{>70}$) and ferroan ($Fo_{<26}$) compositions.

4.5. Sulfide-rich or metal-rich clasts (E)

There are several sulfide-rich or metal-rich clasts in DAG 319. Representative chemical compositions of the minerals in these clasts are shown in Tables 6a, b.

In sulfide-rich lithic clasts (E1), olivine is the major mineral and has normal zoning. A sulfide-rich clast (E1; α32A), 2.1 mm $\times$ 0.6 mm, consists mainly of sulfide and olivine (Fig. 5a); the olivine grains have normal zoning from magnesian (Fo_{83}) to ferroan (Fo_{47}) compositions, and a porous matrix consisting mainly of ferroan olivine laths (Fig. 5b) is similar to the Allende matrix.

In metal-rich clasts (E2), however, olivine is absent. Instead, pyroxenes occur and are magnesian, with mg $>$ 0.98. They are CaO-poor enstatite (CaO $<$ 0.2 wt%, Table 6a). Fine-grained aggregates of metal and silicates sometimes occur in enstatite grains (Fig. 5c), which correspond to a composition of ferroan low-Ca pyroxenes. Therefore, the enstatite in metal-rich clasts may have been produced from more ferroan lithologies by intense reduction. A silica mineral occurs in this type, along with enstatite. A metal-rich clast (E2; α42), 2.5 mm $\times$ 0.6 mm, consists mainly of metal-sulfide, enstatite, and a silica mineral (Fig. 5c). The enstatite is En_{98-99} and very poor in CaO. Sometimes the cores of the enstatite grains are

Table 6a. Chemical compositions of silicate minerals and mesostasis in sulfide- and metal-rich clasts (group E).

Type	E1	E1	E2	E2	E2	E2	E2	E2
Clast	α 32A	α 32A	α 42A	α 42A	α 42A	α 44A	α 44A	δ 4
No.	1998	988	1282	1254	1268	1325	1323	299
Mineral	Ol	Ol	En	Pl	Silica	En	Meso	En
SiO2	40.37	34.54	61.27	62.90	98.16	60.51	71.01	59.44
TiO2	0.00	0.00	0.00	0.00	0.00	0.00	0.00	0
Al2O3	0.00	0.00	0.00	23.04	0.10	0.00	16.89	0.1
Cr2O3	0.25	0.00	0.00	0.00	0.00	0.00	0.00	0
FeO	12.67	39.49	0.51	0.46	0.91	0.34	0.51	0.04
MnO	0.20	0.19	0.00	0.00	0.00	0.03	0.08	0
MgO	46.13	24.22	38.81	0.07	0.03	39.75	5.46	39.66
CaO	0.10	0.22	0.00	5.05	0.00	0.00	0.00	0.2
Na2O	0.07	0.06	0.00	8.82	0.05	0.04	5.08	0.06
K2O	0.00	0.00	0.05	0.27	0.02	0.05	0.90	0
Total	99.79	98.72	100.64	100.61	99.27	100.72	99.93	99.50
mg ratios	0.87	0.52	0.99			1.00	0.95	1.00

Table 6b. Chemical compositions of metal and sulfide in sulfide- and metal-rich clasts (group E2).

Type	E2	E2	E2	E2
Clast	α 42A	α 44A	δ 4	δ 4
No.	M150	M153	M105	M115
Mineral	Pyrrh	Ka	Ka	Pyrrh
Si	0.03	2.83	3.41	0
P	0	0.13	0.14	0
S	36.35	0	0.01	39.02
Cr	2.18	0.02	0	6.98
Mn	0.46	0.01	0	0.48
Fe	58.24	87.74	89.41	50.51
Co	0.1	0.41	0.5	0.03
Ni	0.16	7.46	6	0.23
Total	97.52	98.6	99.47	97.25

fine-grained aggregates of enstatite and tiny metal, corresponding to more ferroan orthopyroxenes (En_{81-86}). This clast contains two small plagioclase grains (An_{36} and An_{24}) (Fig. 5c). Another large metal-rich clast (E2; $\delta4$), 6 mm $\times$ 3 mm, consists of enstatite and a metal-sulfide network (Fig. 5d); the metal is Si-bearing kamacite (Table 6b).

4.6. Chondrules and chondritic fragments (F)

Several complete chondrules, chondrule fragments and chondritic fragments were found in DAG 319. Representative chemical compositions of the minerals in these clasts are shown in Tables 7a, b.

The chondrules (F1) found are barred Ol (Fig. 6a), porphyritic Ol (Fig. 6b), porphyritic Ol and Pyx (Fig. 6c), porphyritic Pyx (Fig. 6d) and radial Pyx (Fig. 6e). Olivines in this type show normal zoning. Pyroxenes and glasses in chondrules are variable and similar to those in ordinary chondrites, although glass in a radial pyroxene chondrule ($\delta7$) is extremely magnesian (Table 7a). It is interesting to note that the mineral compositions of these chondrules differ significantly from the common type 1 chondrules found in all carbonaceous chondrites (McSween, 1977), which are very low in FeO, and the FeO-richer uncommon type II chondrules.

Chondritic fragments (F2) contain olivine, pyroxene, and plagioclase. Olivines in this type often have normal zoning from magnesian cores (up to Fo_{85}) to ferroan rims (down to Fo_{65}), in spite of the occurrence of plagioclase. Pyroxenes are similar in composition and occurrence to those in ordinary chondrites. The plagioclase is interstitial and sodic; $An_{6-10}Or_{6-8}$ in a clast (F2; $\alpha43$) and $An_{10-11}Or_5$ in another clast

Table 7a. Chemical compositions of silicate and oxide minerals, groundmasses and glasses in chondrules and chondrites (group F)

Type	Barred Ol			Porphyritic Ol			Porphyritic Ol-Pyx				Porphyritic En-Di			Radial Pyx				
Clast	α14A	α14A	α14A	α41	α41	α41	α33B	α33B	α33B	α33B	α36B	α36B	α36B	δ7	δ7	γ16	γ16	γ16
No.	43	44	767	76	80	1225	1902	1901	1917	1909	1151	1155	1146	3	362	292	289	290
Mineral	Ol	Opx	Gdm	Ol-core	Ol-rim	Gl	Ol	Opx	Gdm-Pl	Gdm	En	Aug	Gl	En	Gl	Ol	Opx	Gl
SiO2	37.88	56.08	57.96	42.43	37.84	66.87	38.87	57.82	69.64	62.94	59.14	55.87	68.02	58.29	70.89	38.65	56.59	66.64
TiO2	0.00	0.03	0.08	0.00	0.00	0.28	0.00	0.02	0.06	0.21	0.00	0.16	0.45	0.08	0	0	0.04	0.04
Al2O3	0.00	0.04	8.08	0.00	0.00	11.63	0.00	0.11	18.16	15.68	0.05	0.81	17.61	0.38	17.83	0	0.09	19.6
Cr2O3	0.03	0.11	0.38	0.58	0.71	0.09	0.01	0.06	0.02	0.20	0.28	0.80	0.12	0.37	0	0	0.17	0.01
FeO	26.11	15.34	6.40	5.70	24.80	7.91	18.02	10.60	0.39	1.72	0.65	2.55	1.88	0.46	0	23.65	13.5	0.75
MnO	0.46	0.45	0.14	0.22	0.77	0.32	0.23	0.59	0.00	0.00	0.15	0.54	0.08	0.17	0	0.41	0.12	0
MgO	35.65	27.61	12.22	51.94	35.18	1.84	41.33	30.60	0.09	3.70	38.69	22.84	0.89	38.53	1.16	38.08	28.91	0.23
CaO	0.14	0.69	9.42	0.14	0.20	3.20	0.03	0.42	0.17	5.90	0.13	16.46	3.53	0.34	2.13	0.05	0.81	1.93
Na2O	0.00	0.01	4.49	0.03	0.03	5.88	0.00	0.00	10.77	8.38	0.07	0.28	4.90	0.08	6.48	0.04	0.08	10.43
K2O	0.04	0.00	0.31	0.00	0.00	1.25	0.00	0.00	1.66	0.77	0.01	0.00	0.84	0.02	0.94	0	0	1.19
Total	100.31	100.36	99.48	101.04	99.53	99.27	98.49	100.22	100.96	99.50	99.17	100.31	98.32	98.72	99.43	100.88	100.31	100.82
mg ratios	0.71	0.76	0.77	0.94	0.72	0.29	0.80	0.84	0.29	0.79	0.99	0.94	0.46	0.99	1.00	0.74	0.79	0.35

Type	Chondritic Fragment				Chondritic Fragment			
Clast	α43A	α43A	α43A	α43A	β22B	β22B	β22B	β22B
No.	1294	1290	1301	1313	169	180	179	183
Mineral	Ol	Ol	Opx	Pl	Ol	Aug	Pl	Chm
SiO2	37.28	38.20	54.40	65.08	35.39	54.13	64.97	0.20
TiO2	0.00	0.00	0.05	0.00	0.00	0.21	0.00	5.29
Al2O3	0.02	0.02	0.15	20.88	0.04	0.61	21.66	5.76
Cr2O3	0.00	0.71	0.19	0.00	0.02	0.52	0.00	45.89
FeO	28.59	19.49	17.51	0.86	36.24	7.18	0.73	38.57
MnO	0.28	0.16	0.24	0.05	0.28	0.00	0.00	0.20
MgO	32.99	39.07	25.77	0.10	26.12	4.57	0.09	1.72
CaO	0.05	0.33	0.94	2.02	0.19	22.79	2.41	0.02
Na2O	0.00	0.02	0.09	9.60	0.03	0.61	9.74	0.04
K2O	0.00	0.02	0.00	1.07	0.02	0.03	0.86	0.04
Total	99.21	98.02	99.34	99.66	98.33	90.65	100.46	97.73
mg ratios	0.67	0.78	0.72		0.56	0.53		0.07

Table 7b. Chemical compositions of metal and sulfide in a chondrule (group F5).

Type	Radial Pyx	
Clast	γ16	γ16
No.	M101	M102
Mineral	Pyrrh	Tae
Si	0.07	0.05
P	0	0.05
S	36.35	0
Cr	0.24	0.1
Mn	0.02	· 0
Fe	60.42	85.32
Co	0.09	0.6
Ni	0.37	13.17
Total	97.56	99.29

Y. Ikeda, M. Prinz and C. E. Nehru

Table 8a. Chemical compositions of silicate and oxide minerals occurring as isolated minerals (group G).
Asterisk (*) is inclusions in an isolated mineral.

Type	G1	G1	G1	G1	G1	G1	G1	G1	G1	G2	G2	G2	G2	G2	G2	G2	G2
Clast	α23A	α18A	α46A	α36A	α36A	α15A	α15A	α16D	α16D	α20A	α8E	α8E	α14B	α14B	α45A	β7A	β7A
No.	293	188	492	1129	1119	160	166	172	173	818	618	617	148	1027	495	64	59
Mineral	Ol	Ol	Ol	Ol-core	Ol-rim	Ol-core	Ol-rim	fOl	Chm*	Opx	Opx	Pig	fOpx	Chm*	Aug	Aug	Ol*
SiO2	41.98	42.97	40.14	38.93	42.49	39.50	42.74	35.89	0.01	57.47	56.87	55.29	47.34	0.00	54.12	54.10	40.06
TiO2	0.03	0.05	0.01	0.00	0.00	0.00	0.01	0.00	5.91	0.03	0.00	0.00	0.41	3.05	0.30	0.28	0.00
Al2O3	0.00	0.02	0.00	0.00	0.03	0.00	0.00	0.00	5.32	0.76	0.06	0.41	0.27	5.61	1.76	1.41	0.01
Cr2O3	0.01	0.02	0.43	0.65	0.04	0.78	0.60	0.01	43.16	1.32	1.06	0.94	0.20	56.97	1.56	1.12	0.41
FeO	0.16	0.12	11.71	17.28	0.25	19.42	2.87	33.34	40.51	5.24	8.28	12.12	36.85	25.84	4.17	4.14	12.01
MnO	0.23	0.06	0.51	0.40	0.12	0.35	0.35	0.43	0.27	0.65	0.39	0.56	0.98	0.63	0.41	0.37	0.43
MgO	56.09	57.15	46.27	41.62	56.82	40.45	53.84	29.30	1.85	32.69	29.67	23.95	9.52	5.40	19.78	20.28	45.92
CaO	0.04	0.08	0.28	0.29	0.10	0.27	0.28	0.09	0.03	2.21	2.22	6.37	2.53	0.00	18.69	17.84	0.38
Na2O	0.03	0.01	0.02	0.04	0.03	0.00	0.00	0.00	0.00	0.09	0.00	0.05	0.03	0.00	0.29	0.17	0.00
K2O	0.03	0.00	0.00	0.03	0.01	0.00	0.00	0.00	0.00	0.00	0.00	0.05	0.00	0.00	0.01	0.00	0.15
Total	98.60	100.48	99.37	99.24	99.89	100.77	100.69	99.06	97.06	100.46	98.55	99.69	98.13	97.50	101.09	99.71	99.37
mg ratios	1.00	1.00	0.88	0.81	1.00	0.79	0.97	0.61	0.08	0.92	0.86	0.78	0.32	0.27	0.89	0.90	0.87

Table 8b. Chemical compositions of metal and sulfide occurring as isolated minerals (group G).

Type	G3	G3	G3	G3	G3	G3
Clast	α5C	β34A	β34A	α22A	α35A	β32A
No.	1357	48	40	8	70	51
Mineral	Pl	Pl	Aug*	Pl	Pl	Pl
SiO2	45.64	45.12	53.05	57.04	67.30	65.78
TiO2	0.00	0.00	0.01	0.00	0.05	0.04
Al2O3	34.53	34.52	3.25	26.84	20.07	20.35
Cr2O3	0.00	0.00	0.98	0.00	0.00	0.00
FeO	0.36	0.00	0.81	0.00	0.18	0.22
MnO	0.05	0.00	0.12	0.00	0.13	0.00
MgO	0.30	0.31	17.51	0.17	0.00	0.14
CaO	18.79	18.93	22.80	10.06	2.59	2.07
Na2O	0.87	0.74	0.21	6.26	10.71	10.16
K2O	0.00	0.02	0.05	0.00	0.22	0.50
Total	100.54	99.64	98.79	100.37	101.25	99.26
mg ratios			0.97			

Type	G9	G9	G9	G9	G9	G9	G9	G9	G9	G9	G9
Clast	α6C	α8F	α8F	α8G	α18F	α18F	α20D	α20D	α5E	α5E	α5E
No.	M84	M67	M79	M80	M88	M91	M97	M98	M111	M112	M113
Mineral	Ka	Ka	Tr	Sulfide	Ta	Tr	Tr	Pent	Schreib	Ka	Barring
Si	5.48	0.05	0.07	0.00	0.04	0.02	0.01	0.02	0.83	11.22	1.21
P	0.41	0.81	0.00	0.00	0.00	0.01	0.00	0.00	15.71	0.13	20.37
S	0.00	0.00	36.95	37.40	0.02	36.43	37.39	34.44	0.02	0.00	0.02
Cr	0.05	0.00	0.87	4.39	0.04	0.00	0.01	0.03	2.45	0.47	4.75
Mn	0.00	0.00	0.10	0.83	0.00	0.00	0.00	0.00	0.10	0.00	0.44
Fe	89.29	96.00	59.01	54.09	70.71	61.54	60.42	37.00	77.70	82.49	66.08
Co	0.56	0.19	0.10	0.16	1.12	0.05	0.09	0.46	0.24	0.61	0.65
Ni	4.00	1.53	0.06	0.26	27.53	0.09	0.56	27.44	3.30	4.89	4.48
Total	99.79	98.58	97.16	97.13	99.46	98.14	98.48	99.39	100.35	99.81	98.00

(F2; β22B). It is very similar in composition and occurrence to that in ordinary chondrites. A chondritic fragment (Fig. 6f; α43), $800\,\mu \times 200\,\mu$, consists of ferroan olivine (Fo_{78-66}), orthopyroxene, and sodic plagioclase (An_{6-10}).

4.7. Isolated mineral clasts (G)

Many isolated mineral clasts occur in DAG 319, and most are fragments of larger lithic clasts. Representative chemical compositions of the minerals in these clasts are shown in Tables 8a, b.

Large olivine clasts (G1-1; Fig. 7a) appear to be related to type I or type II ureilitic lithic clasts (A1, A2), although the source of the forsterite (G1-3; Fig. 7b) is problematic; it might have a genetic relationship with the magnesian Ol-rich clasts (A3) or the fine-grained Fo-rich clasts (B3). Isolated pyroxene clasts (G2; Fig. 7c) appear to be related to pyroxene-bearing lithologies such as ureilitic clasts, especially to type I and II ureilites. Enstatite (G2-4) is a persistent isolated mineral clast type, often associated with forsterite ($Fo_{>99}$). This seems to represent a small percentage of a highly reduced rock type; it might relate genetically with the metal-rich lithic clasts (E2). An isolated pyroxene clast (G2-3; α8E; Fig. 7d), $200\,\mu$ across, consists of orthopyroxene host and pigeonite lamellae. The widths of the lamellae are less than $2\,\mu$ and the distance between the lamellae is a few microns. Pigeonite blebs, up to $10\,\mu$ across, are found in the peripheral portion of the grain. Pyroxenes with exsolution lamellae are very rare in common monomict ureilites.

Isolated plagioclase (G3) is common in DAG 319, and it is sometimes very large, from $100\,\mu$ up to 5 mm, although the number of clasts found is small. Compositions range widely from anorthite (An_{99}) to albite (An_5), and it is not clear whether these represent distinct groupings or are a continuum. The large calcic plagioclases may represent fragments from gabbroic lithologies or phenocrysts in porphyritic lithologies. A large plagioclase clast (α22; An_{46-49}), about 5 mm across, contains many magmatic inclusions, about $50-200\,\mu$ across (Fig. 7e). These magmatic inclusions consist mainly of sodic plagioclase, augitic pyroxene, and rare mesostasis. They will be discussed elsewhere in a companion paper.

Chromite, ilmenite, apatite, whitlockite, sulfides, and metallic clasts, all of which occur as isolated minerals, are also found in lithic clasts, suggesting they are derived by disaggregation. Si-bearing kamacite, suessite, perryite and bladed graphite also occur in DAG 319. An isolated metallic grain (α5E; Fig. 7f) consists of schreibersite, barringerite, and Si-bearing kamacite.

5. Mineralogy

5.1. Olivine

Olivine occurs in the lithic and mineral clasts of all groups, and all are shown in Fig. 8, where CaO, MnO and Cr_2O_3 are plotted against $Fe/(Mg+Fe)$. Olivine is the main phase in the coarse-grained mafic lithic clasts and ranges from Fo_{74-100}. The olivine grains in type I ureilitic clasts (A1) have reverse zoning, with ferroan cores (Fo_{74-80}) and magnesian rims ($Fo_{>95}$). On the other hand, olivines in the type II
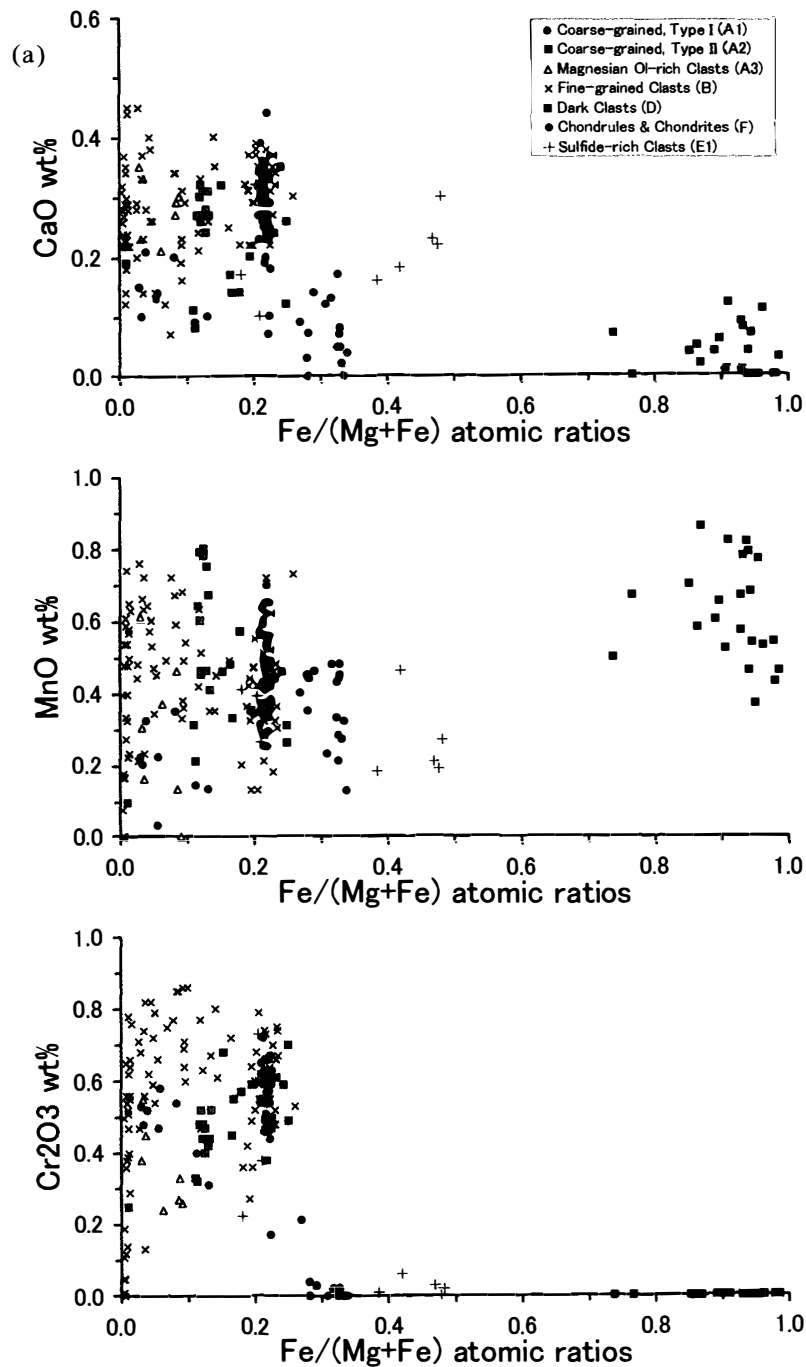
Fig. 8. Olivine compositions in the DAG 319 polymict ureilite. (a) olivines in lithic clasts; Type I (A1), Type II (A2), magnesian Ol-rich clasts (A3), fine-grained clasts (B), dark clasts (D), chondrules & chondrites (F), and sulfide-rich clasts (E1), and (b) olivines occurring as isolated mineral clasts (G1).

ureilitic clasts (A2) have a range of compositions from Fo_{85-90}; there is little or no reverse zoning in the rims because there is little or no associated carbon. Olivines in the magnesian Ol-rich clasts (A3) have a range of compositions from Fo_{90-98} in the cores, and remarkable reverse zoning up to Fo_{100}. Figure 8a shows that olivines
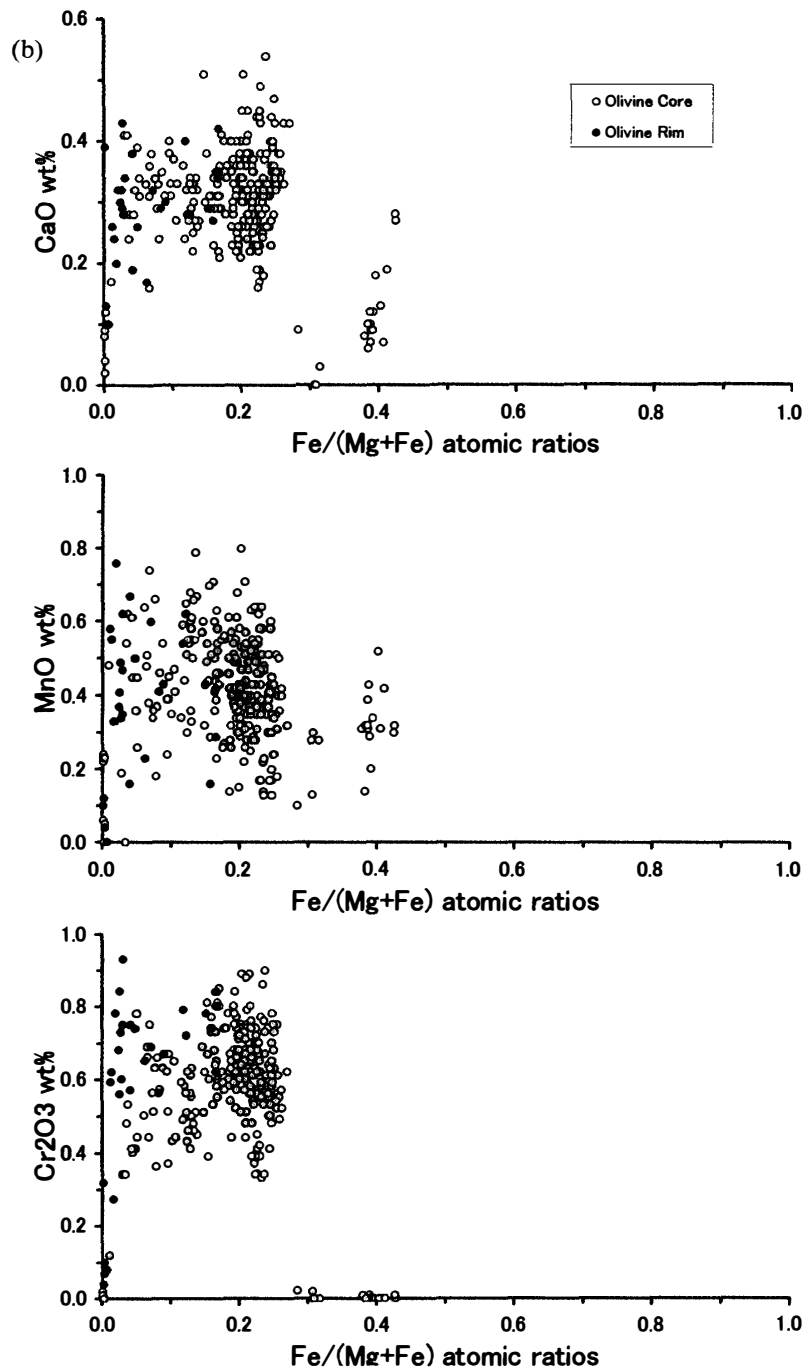
Fig. 8.   (Continued).

in type I, type II, and magnesian ureilitic clasts have high CaO, MnO and Cr_2O_3
contents typical of ureilitic olivine. Olivines in the fine-grained mafic lithic clasts
(B) are generally more reduced because of their smaller grain size. On the other
hand, the fayalitic olivines in the dark clasts (D) are depleted in Cr and Ca, but
magnesian olivines in these clasts are rich in Cr and Ca. The sulfide-rich clasts (E1)
also have olivines poor in Cr_2O_3. Olivines in chondrules and chondritic fragments
(F) are different from those in ureilitic lithologies and poorer in CaO and Cr_2O_3

except for magnesian ones.

Figure 8b shows the isolated olivine clasts and clearly indicates that they are mainly from type I ureilites and, to a lesser extent, from type II and magnesian ureilites. There are also some Fe-rich olivine grains with mg$=0.5-0.7$ which have no Cr. They may be derived from sulfide-rich clasts (E1) or chondrules and chondritic fragments (F).

As shown in Fig. 8, it is clear that the Cr_2O_3 contents of magnesian olivines are higher than those of ferroan olivines. This may be explained by formational redox conditions; magnesian olivines were produced under reduced conditions where most Cr was divalent, whereas ferroan ones formed under oxidized conditions where most Cr was trivalent.

5.2. Pyroxenes

Both low-Ca and high-Ca pyroxenes occur in DAG 319 and are plotted in Fig. 9. They mainly have a range of mg ratios from 0.25 to 1.00, but pyroxenes with mg ratios less than 0.70 are minor.

The MnO and Cr_2O_3 contents of all pyroxenes are plotted against the Fe/(Mg+Fe) atomic ratios (hereafter, fe ratios) in Fig. 10. Generally speaking, the Cr_2O_3 contents of pyroxenes are higher for high-Ca pyroxenes than for low-Ca pyroxenes. The Cr_2O_3 contents of low-Ca pyroxenes with fe <0.20 increases with FeO content; the Cr_2O_3 of low-Ca pyroxenes is about 0 wt% at fe$=0.00$ and about 1 wt% at fe$=0.20$ (Fig. 10). This may be due to reduction, in which Cr changes from Cr^{+2} to metallic Cr or it becomes a chalcophile element. On the other hand, the Cr_2O_3 content of low-Ca pyroxenes having fe >0.25 are low (Fig. 10), and their crystalli-
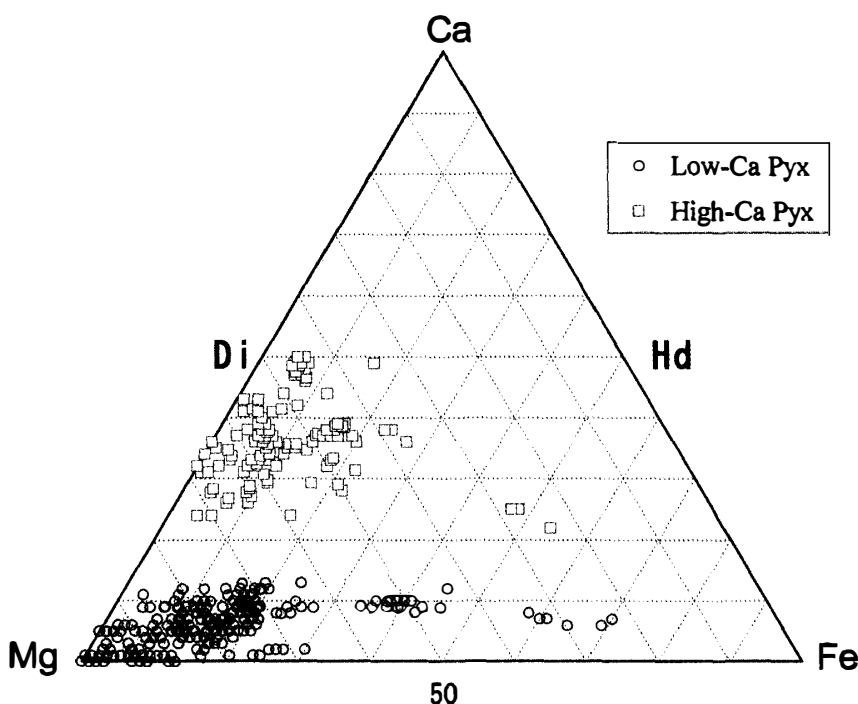
Fig. 9.   Ca-Mg-Fe atomic compositions of pyroxenes in the DAG 319 polymict ureilite.
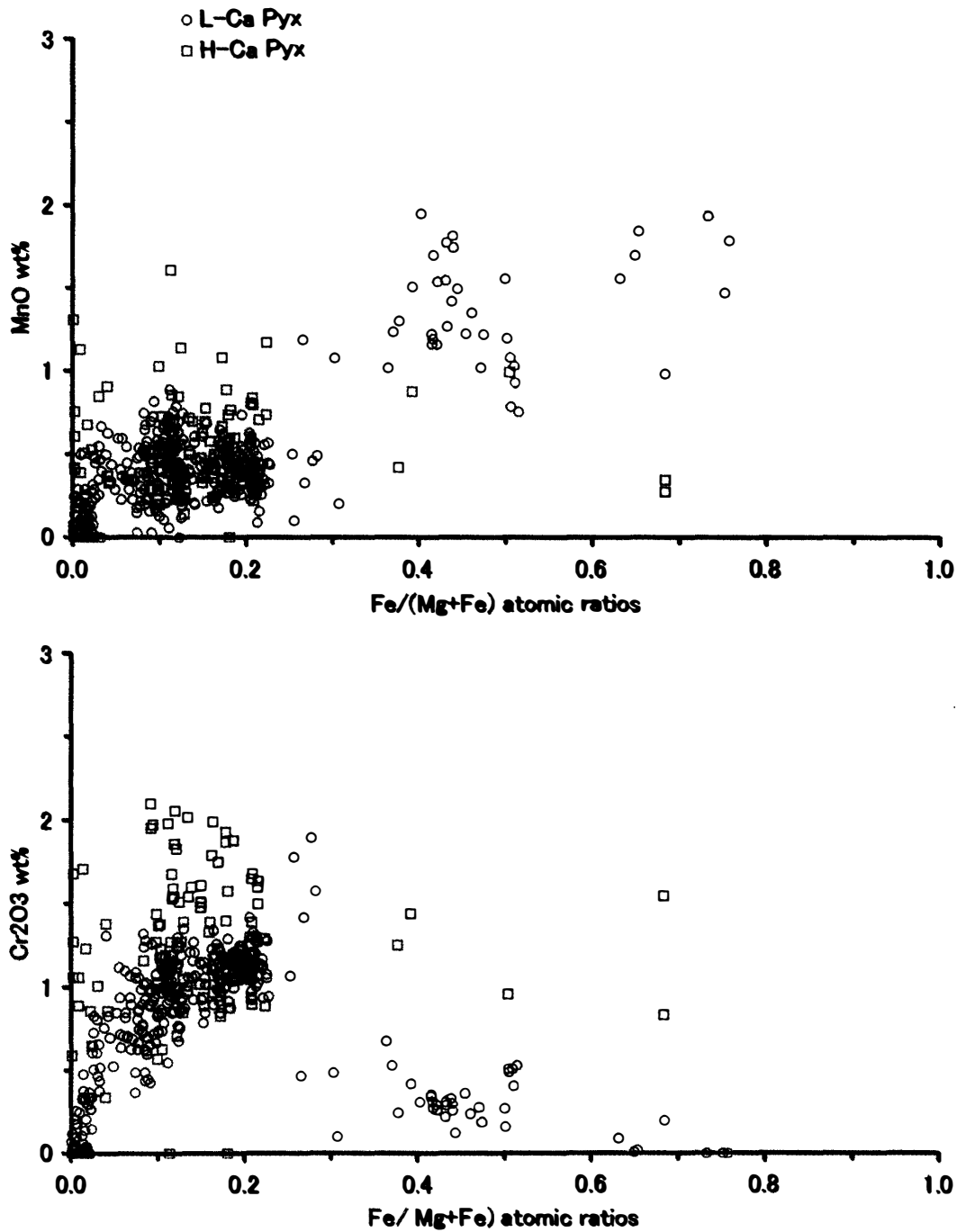
Fig. 10. Cr_2O_3 and MnO contents of pyroxenes in the DAG 319 polymict ureilite.

zation may have taken place under more oxidizing conditions, where Cr is mainly trivalent and chromite occurs commonly. The MnO content of pyroxenes increases with fe ratio (Fig. 10) and this may be explained by the fact that Mn is mostly divalent, although it becomes a metallic or chalcophile element under extremely reducing conditions.
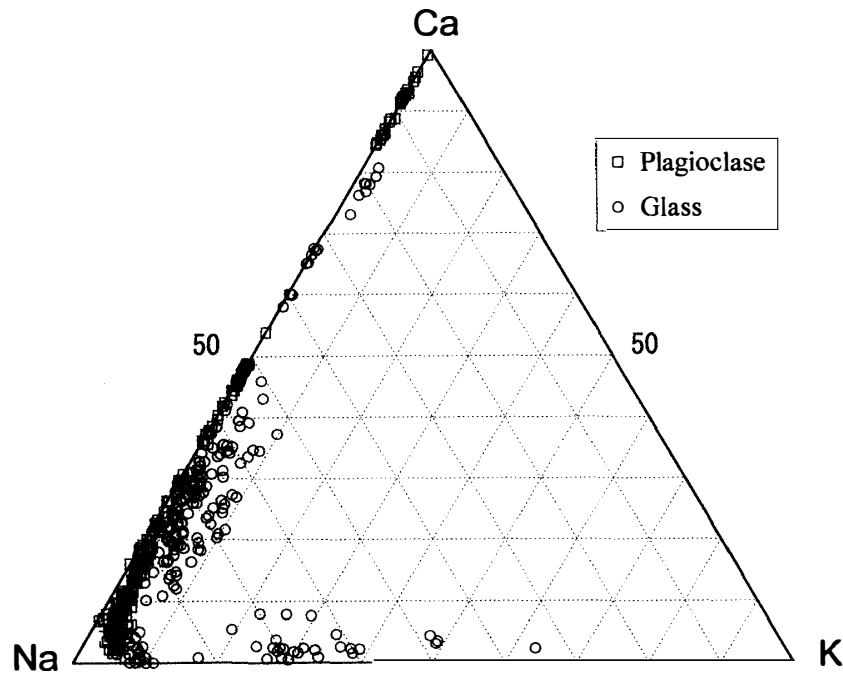
Fig. 11.   Ca-Na-K atomic compositions of plagioclase and glass in the DAG 319 polymict ureilite.

5.3.   Plagioclase and glass

Plagioclase does not occur in coarse-grained mafic lithic clasts (A), and is very rare in the fine-grained mafic lithic clasts (B). Plagioclases are very common in the felsic group (C), but are very rare in dark clasts (D) and sulfide-rich and metal-rich lithic clasts (E). All of the plagioclase found in DAG 319 is plotted in Fig. 11 and shows a wide compositional range from An_{0-100}. There appears to be a compositional hiatus between An_{65} and An_{80}.

Glass is found in the fine-grained mafic lithic clasts (B), felsic clasts (C) and chondrules (F), and all the glass is plotted in Fig. 11. In comparison to plagioclase, glasses are less calcic and more potassic in composition. Some are enriched in K_2O contents.

5.4.   Chromite, ulvospinel, magnetite, and ilmenite

Spinel group minerals and ilmenite in DAG 319 are plotted in Fig. 12. Chromite, ulvospinel, and ilmenite occur in porphyritic felsic clasts (C1, Table 4a). Chondritic fragments (F) also contain chromite (Table 7a). Isolated grains of ferroan olivine ($mg = 0.61$) include small grains of chromite (Table 8a), and small chromite grains occur in an isolated grain of ferroan orthopyroxene ($mg = 0.32$, Table 8a). An isolated grain with a composition between chromite and magnetite is plotted in Fig. 12. Ilmenite occurs as microphenocrysts set in the groundmass of porphyritic felsic clasts, and also as an isolated mineral. A small grain of ulvospinel occurs in the groundmass of a porphyritic felsic clast. Magnetite grains are common in all dark clasts (D). They are usually rounded or subrounded grains in the matrix of the clasts, and their shape is in contrast with the elongated euhedral (rectangular) shape of the coexisting pyrrhotites. Magnetite occurs rarely as
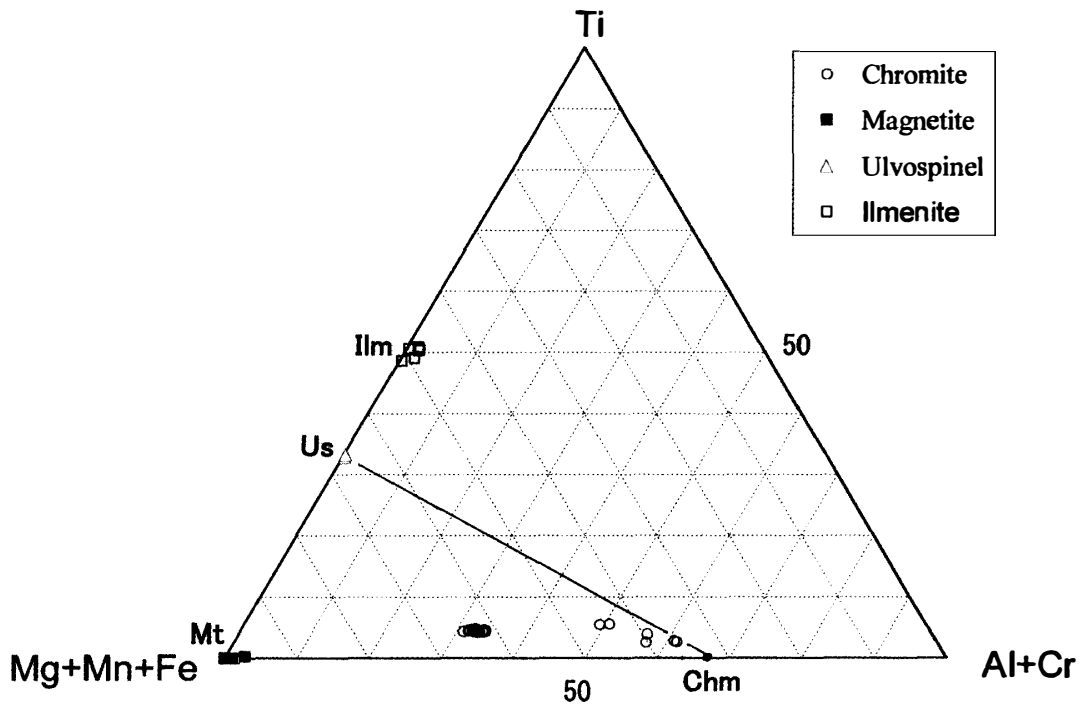
Fig. 12. *Ti-(Mg + Mn + Fe)-(Al + Cr) atomic compositions of chromite, ulvospinel, magnetite, and ilmenite in the DAG 319 polymict ureilite.*
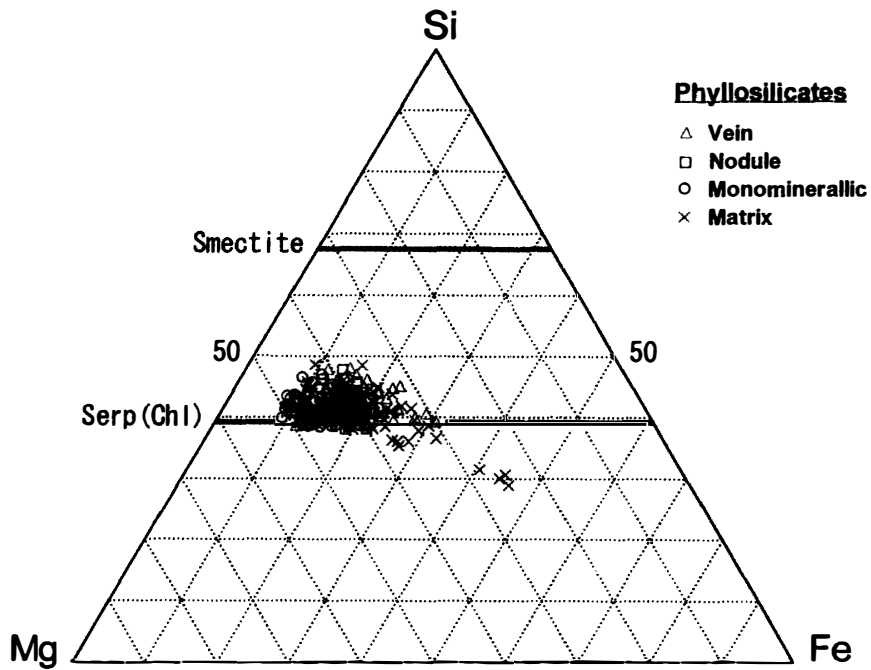
Fig. 13. Chemical compositions of phyllosilicates and matrix in dark clasts are plotted in Si-Mg-Fe atomic ratios.

framboids (Fig. 4h) in the matrix of the dark clasts. It is composed of pure magnetite, with no TiO_2.

5.5. Phyllosilicates

Phyllosilicates are the main phase of all dark clasts (D), and occur as matrix, as vein and nodule minerals (Figs. 4c, g), and as a monomineral set in the matrix. The chemical compositions of the phyllosilicates are plotted in Fig. 13, and they are probably mixtures of serpentine (or chlorite) and minor smectite. The matrix of the dark clasts consists of a fine-grained mixture of phyllosilicates, Ca-bearing phases such as phosphates and carbonates, and opaque minerals such as magnetite and sulfides.

Phyllosilicates in the Fa-bearing clasts (D2) have similar compositions to those in the Fa-free clasts (D1) and plot in the same compositional range, except that the former plot in a range slightly richer in SiO_2.

5.6. Phosphates and carbonates

Phosphates occur in porphyritic felsic clasts (C1) and in dark clasts (D1). They are whitlockite and apatite in the porphyritic felsic clasts (C1); small grains of whitlockite are included in phenocrysts of plagioclase and pyroxene, where apatite microphenocrysts are found in groundmass glass. The occurrences of the phosphates in the porphyritic clasts (C1) suggest that whitlockite crystallized in the early stage and apatite precipitated in the late stage of the clast crystallization.

Carbonates occur in dark clasts (D1), and are mainly dolomite and magnesite. The MnO contents (Table 5a) of carbonates, as well as phosphates, are plotted in Fig. 14. The magnesites contain high MnO, up to 7 wt%, but dolomites contain 1–4 wt% MnO. Calcite veins, which were produced by terrestrial weathering and are not shown in Fig. 14, are free from MnO.
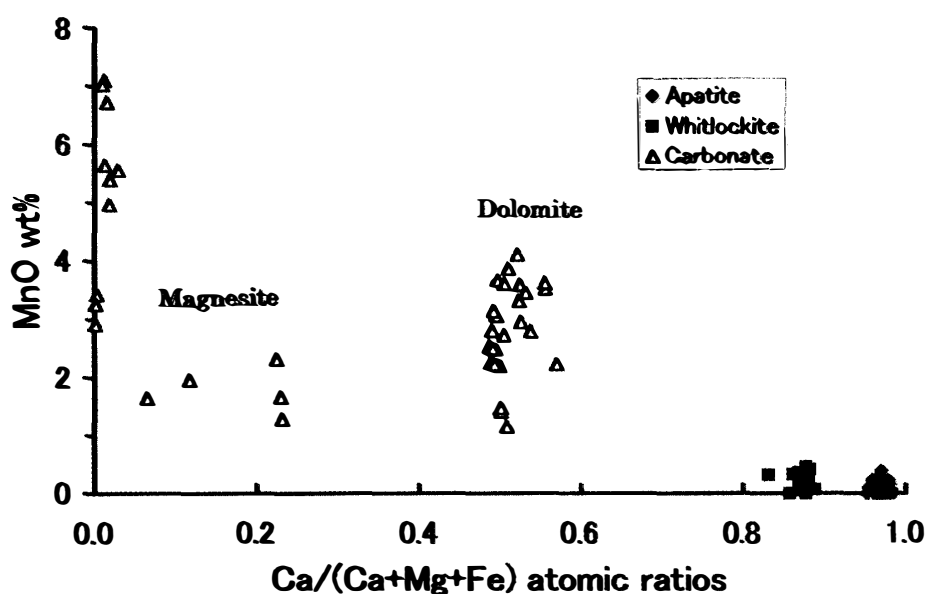
Fig. 14. MnO contents of carbonates (magnesite and dolomite) in dark clasts and phosphates in dark clasts and porphyritic felsic clasts in DAG 319.
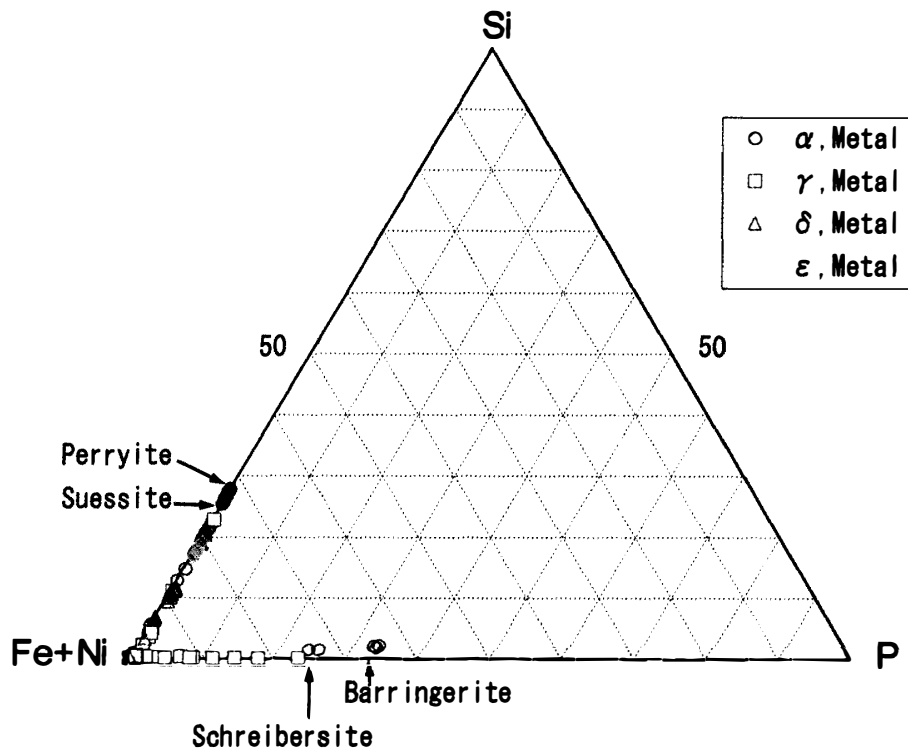
Fig. 15.   Si-(Fe + Ni)-P atomic compositions of metal in the DAG 319 polymict ureilite.   (α, Metal) in the legend is metallic phases occurring in a thin section 4963-1 (α), and so on.

5.7.   Metal, silicide, phosphide, and sulfide

The compositions of metal in DAG 319 are shown in Fig. 15. Si-bearing metal grains are Si-rich kamacite, suessite (Fe_3Si), perryite (Fe_5Si_2). P-bearing metal grains are P-bearing kamacite, schreibersite (Fe_3P), and barringerite (Fe_2P). Metal grains in the type I ureilitic clasts (A1) are mainly Si-rich kamacite, whereas those in type II ureilitic clasts (A2) are mainly P-bearing kamacite and schreibersite (Table 2b).

Metallic phases occurring in the fine-grained mafic lithic clasts (B1) are Si-rich kamacite and suessite (Table 3b), suggesting that these clasts were produced under intensely reduced conditions. Sulfides in the fine-grained clasts (B1, B2) are pyrrhotite and daubreelite ($FeCr_2S_4$).

Metal grains do not occur in the porphyritic felsic clasts (C1). Metal surrounded by sulfide is found in pilotaxitic clasts (C2), and it is taenite (Table 4b). Metal never occurs in the dark clasts (D), but sulfide grains, pyrrhotite and pentlandite (Table 5b), are common. Metal grains in metal-rich clasts (E2) are Si-rich kamacite, and sulfides are Cr-bearing sulfides (Table 6b). Metal grains in chondrules and chondritic fragments (F) are rare, but a taenite-sulfide grain in a chondritic fragment was analyzed (Table 7b).

6.   Discussion

There are abundant clast types in DAG 319, and the complexity and variety of
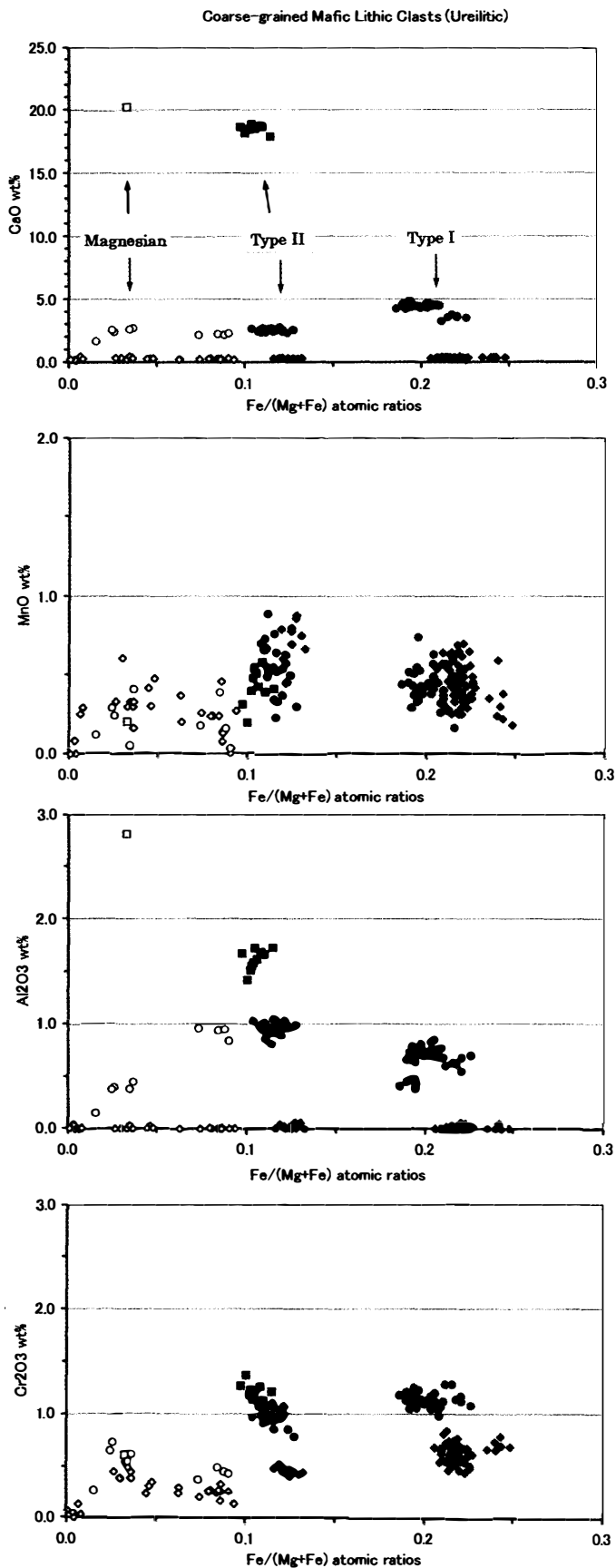
Fig. 16. CaO, MnO, Al₂O₃, and Cr₂O₃ contents of olivine (diamonds), pigeonite or orthopyroxene (circles), and augite (squares) in the coarse-grained mafic (ureilite) lithic clasts, plotted against their Fe/(Mg +Fe) atomic ratios. Type I (blue), Type II (red), and magnesian Ol-rich (yellow) lithologies.

the lithic and mineral clasts, as evidenced by Table 1, makes it difficult to relate all of the fragments to any single coherent petrologic process. Therefore a variety of processes must be invoked. In spite of this diversity we are undertaking an even more extensive survey of the polymict ureilites, which will include a reevaluation of the clasts in Nilpena and North Haig. We shall use these new data to test this classification and also look for critical clasts which may help clarify the relationships and petrogenesis of the different clast types.

The coarse-grained mafic lithic clasts (A) are the main type, and the chemical compositions of the constituent minerals of type I, type II and magnesian ureilitic clasts are shown in Fig. 16. The mineral compositions of type I ureilitic clasts are very similar to those in common monomict ureilites (Goodrich, 1992), and those of type II ureilitic clasts are very similar to those in the unusual monomict ureilites Hughes 009 and FRO 90054 (Goodrich *et al.*, 1999a, b; Tribaudino *et al.*, 1997). In addition to the fact that type II ureilitic clasts are more magnesian than type I clasts, the former are more depleted in carbon components, are nearly free from metal-sulfide network, and contain high-Ca pyroxene more abundantly than the latter. Metallic phases in type II ureilites contain phosphorus, whereas those in type I ureilites contain silicon. The most remarkable difference between type I and type II ureilite clasts is that olivine and orthopyroxene grains in type II clasts contain many magmatic inclusions, whereas type I clasts have none. Type II ureilitic clasts probably had a petrogenesis quite different from that of type I clasts.

Magnesian ureilitic clasts contain magnesian olivine as the main constituent, and the olivine grains have reduction rims due to carbon. They may have experienced reduction in a similar way to that of type I clasts, and are free of magmatic inclusions. Their petrogenesis was probably similar to that of type I clasts.

Since plagioclase-bearing lithic clasts in ureilites are rare, being found only in the polymict ureilites, their relationship to the ureilitic clast types is of great interest. The relationship of at least some of the plagioclase to the ureilitic clasts will be examined by studying the magmatic inclusions in a large plagioclase clast (An$_{47}$, G3.2), described above. The melt inclusions in the olivines and orthopyroxenes in type II ureilite clasts will also be used to determine the composition of the melts involved in the crystallization of these phases.

Oxygen isotope analyses of minerals in these clasts are crucial to an understanding of their relationships and is currently being pursued (Kita *et al.*, 1999). Clearly, polymict ureilites represent one of the best opportunities to develop a better understanding of the origin of ureilites.

6.1. Reduction

Reduction is a very important process for the formation of the coarse-grained and fine-grained mafic lithic clasts (A, B), as well as the metal-rich clasts (E2). Olivine grains in type I ureilitic clasts (A1) have reverse zoning on their rims, a well known feature of the common monomict ureilites. Reduction equations for this phenomenon have been presented by many authors (*e.g.*, Berkley *et al.*, 1976;

Berkley and Jones, 1982; Goodrich, 1992). These authors argue that the Fe_2SiO_4 component of the olivine was reduced by carbon to metallic Fe and SiO_2, and the reduction equation is:

$$Fe_2SiO_4 + 2C \longrightarrow 2Fe + SiO_2 + 2CO , \qquad (1)$$

where the CO component of the products was lost from the ureilite system. A major problem with this reaction is the lack of a SiO_2 component. If monomict ureilites contained interstitial melts, then the SiO_2 component may have gone into those melts (Ikeda, 1999). But, if interstitial melts in monomict ureilites are negligible, the proposed SiO_2 must remain in the reduced olivine rims as enstatite grains or a silica mineral. However, the reduced olivine rims of the common monomict ureilites, as well as the type I ureilitic clasts in DAG 319, do not contain any silica minerals. Instead, small amounts of enstatite are observed in the reduction rims, but the amount is very small. Therefore a new explanation for the absence of SiO_2 in the reduced rims of olivines is needed.

If reduction is more intense than that in equation (1), then SiO_2 may be reduced to metallic Si. The following equation is essentially the same as that proposed by Berkley and Jones (1982);

$$Fe_2SiO_4 + 4C \longrightarrow 2Fe + Si + 4CO , \qquad (2)$$
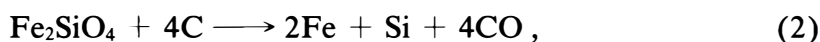
where Si of the product is metallic, and forms Si-rich metal with 2Fe of the product, as well as with additional metallic Fe. As shown above, type I ureilitic clasts (A1) contain abundant Si-bearing metal, and equation (2) is the appropriate one for their formation. Thus, the type I ureilitic lithology may have experienced intense reduction, as expressed by equation (2), after the consolidation of this lithology with the associated carbon. Reduction of the olivine rims in common monomict ureilites may also be the result of equation (2), although some may be by equation (1).

The fine-grained mafic lithic clasts (B1, B2) also experienced similar reduction, as their metallic phases are Si-bearing kamacite and suessite (Table 3b). Thus, their reduction may be expressed by equation (2).

Type II ureilitic clasts (A2) contain very small amounts of metal, and they contain P-bearing metallic phases such as schreibersite (Table 2b). The type II ureilitic lithology was probably produced from silicate magmas as cumulates, under moderately reducing conditions, whereby a small amount of metallic P may have precipitated. But the SiO_2 components of the magmas were not reduced to metallic Si.

Metal-rich clasts (E2) may have been produced from more ferroan lithologies, by reduction, to produce enstatite and a silica mineral. Metallic phases in the metal-rich clasts (E2) are Si-bearing kamacite. Si-bearing metallic melts probably intruded into the more ferroan lithologies and, with decreasing temperatures, supplied Si to produce enstatite and a silica mineral with oxygen.

6.2. Reverse zoning of phenocrysts and magma mixing

The felsic lithic clasts (C) have igneous lithologies and could represent at least some of the missing ureilite basaltic melt components or their differentiates. The porphyritic felsic clasts (C1) are the main lithology, but they are olivine-free. Since the missing basaltic melts should be saturated with olivine components, the porphyritic type cannot represent the missing basaltic melts themselves. But they can be their differentiates or related melts.

The phenocrysts of both plagioclase and pyroxene phenocrysts in some of the porphyritic felsic clasts have reverse zoning, as already shown in the foregoing sections. The two kinds of reverse zoning of the phenocrysts are very sharp and probably formed at the same time (Figs. 3c, d). If the porphyritic felsic clasts contained volatile components such as H_2O, this zoning could have been produced by rapid loss of the volatiles. However, these porphyritic clasts do not contain any hydrous minerals or bubbles, suggesting they were nearly dry. Therefore, the zoning cannot have been caused by the loss of volatiles.

Alternatively, the two kinds of reverse zoning of the phenocrysts in the porphyritic felsic clasts can be explained by magma mixing processes. A more-differentiated magma may have crystallized phenocrysts of ferroan pyroxene and sodic plagioclase, and another aphanitic, less-differentiated, magma, more calcic and reduced, may have mixed with the former melt. This magma mixing may have produced the two kinds of reverse zoning at the same time. During the magma mixing, the phenocrysts were corroded and lost their original euhedral forms. This resulted in the corroded core outlines of the phenocrysts (Figs. 3c, d). The more magnesian pyroxene and more calcic plagioclase crystallized on the corroded phenocrysts to form magnesian mantles and calcic plagioclase rims surrounding the cores.

6.3. Dark clasts and dark inclusions in CV chondrites

Dark clasts (D) are common in the DAG 319 polymict ureilite. They consist mainly of phyllosilicates and magnetite, as well as sulfides and carbonates. The dark clasts are similar in appearance to the dark inclusions found in CV3 carbonaceous chondrites such as Allende (Johnson *et al.*, 1990), but differ from them in some respects. The dark clasts in DAG 319 have no chondrules whatsoever, whereas some of the dark inclusions in CV3 chondrites have chondrules. Another difference is the presence of anhydrous minerals such as forsterite, rhyolitic glass, and ureilitic fragments, which are not normally found in the CV3 dark inclusions. Some Fa-free dark clasts (D1) contain phyllosilicate veins (Figs. 4b, c, d), within the clasts only, suggesting that hydration took place on their parent body. These clasts commonly also have phyllosilicate nodules (Fig. 4g), which appear to have been produced on their parent body, then broken up, and incorporated into the dark clasts. These veins and nodules do not occur in dark inclusions in CV3 chondrites.

The Fa-bearing dark clasts (D2) contain a few small basaltic igneous lithic fragments (Fig. 4i). These igneous fragments experienced weak hydration and the formation of magnetite in the groundmass. This hydration probably took place at

the same time as that of the host matrix in the dark clasts (D2). The Fa-bearing dark clasts were probably anhydrous originally, and included anhydrous basaltic igneous lithic fragments. These clasts experienced weak hydration, as well as the formation of fayalitic olivine and magnetite in the matrix. The precursors of the common monomict ureilites may also have been anhydrous chondritic materials (Ikeda, 1999), but it is not clear that the Fa-bearing dark clasts (D2) or their equivalents were the precursors of ureilitic lithologies. The relationship of the dark clasts to the ureilites is uncertain, and further detailed studies of this question are planned.

6.4. Chondrules and chondritic fragments and projectiles

There are obvious chondrules and chondritic fragments found in DAG 319 (Fig. 6). These chondritic fragments could be remnants of projectiles which bombarded the polymict ureilite parent body. The chondrule and chondritic fragments have olivine compositions which are mainly mg=0.70–0.80, although some are more Fe-rich (mg=0.56); some olivine cores are more Mg-rich (mg > 0.80). They do not resemble the common Mg-rich type I chondrules of most carbonaceous chondrites, and are more similar to those in ordinary chondrites and sometimes even R chondrites. The chondrules and chondritic fragments contain glass or groundmass with variable compositions ranging from calcic to sodic plagioclase (Table 7a), and are depleted in metal and sulfide components. The petrologic type of the fragments appears to be 3–4.

The olivine compositions are poor in CaO or Cr_2O_3 in comparison to those of typical ureilitic olivines (Table 7a), suggesting that the chondrules and chondritic fragments are foreign materials. We suggest that they are probably projectile materials which collided with the surface of the DAG parent body, helping to produce the regolithic breccia present on the surface.

6.5. Equilibrium temperatures of the lithic clasts

It is important to know the equilibrium crystallization temperatures of the pyroxenes in the different types of clasts in DAG 319 because they constitute a major part of the evolutional history. These temperatures have been obtained by the use of the two-pyroxene geothermometer (Lindsley and Andersen, 1983). In this case, the augite gives a better temperature estimate for equilibration than the coexisting orthopyroxene or pigeonite, and the uncertainty is about 50°C (Lindsley and Andersen, 1983).

The type I ureilitic clasts consist mainly of olivine and pigeonite, and their equilibrium temperatures are not known because they lack low-Ca pyroxene. However, the crystallization temperatures of a similar common monomict ureilite, Asuka-881931, appears to be greater than 1300°C (Ikeda, 1999), suggesting a high temperature origin for the type I ureilites. On the other hand, the type II ureilitic clasts are Ol-Opx-Aug assemblages, with homogeneous augite and orthopyroxene grains that coexist stably. The temperatures obtained for the augite grains in two type II clasts (γ1 and ζ1) are 1250–1200°C. An isolated augite clast (α45A),

which contains a small grain of orthopyroxene with mg=0.89, seems to be an isolated fragment of type II ureilite, and this augite gives a temperature of about 1230°C. These temperatures are consistent with the results of the crystallization temperatures of augites obtained in the augite-bearing monomict ureilites, which were about 1250°C (Takeda *et al.*, 1989).

The fine-grained mafic lithic clasts (B1, B2) sometimes contain augite grains, in addition to orthopyroxene and/or pigeonite grains, and these augite grains give crystallization temperatures from higher than 1300°C to 1250°C. This is consistent with the Mn-Fe correlation of reduced olivines in the ALHA-77257 monomict ureilite that took place at about 1275°C (Miyamoto *et al.*, 1993).

The felsic clasts are fragments of igneous rocks and two pyroxenes are contained in some types of clasts (C1, C2, C3). The porphyritic type (C1) contains pyroxene phenocrysts, which are pigeonite and/or augite, and they sometimes have zoning from ferroan pigeonite cores to magnesian augite rims. In the case of a porphyritic clast (α34, Figs. 3b, c) the mg ratio of the pyroxene phenocrysts is 0.57–0.59 for the pigeonitic cores and 0.73–0.76 for the augite rims. The temperatures of the augite rims, just in contact with the pigeonite cores, are about 1140–1230°C.

Pilotaxitic clasts (C2) contain small pyroxene grains between the plagioclase laths (Fig. 3h), and the pyroxenes often have zoning from pigeonitic cores (mg = 0.91–0.93) to augite rims (mg=0.91–0.95). Temperatures obtained for the augites in contact with pigeonite cores are 1210–1230°C. A magnesian glassy clast (C3-1, α8A, Fig. 3i) contains microphenocrysts of enstatite (mg >0.99) and feathery augite (mg >0.99), and the temperatures obtained for the feathery augite are about 1300°C. This glassy type may be a candidate for the aphanitic magma discussed above for the magma mixing process. A ferroan glassy clast (C3-2, α16A, Fig. 3j) contains pyroxene phenocrysts which are normally zoned from an orthopyroxene core (mg=0.75–0.80) to pigeonite rim (mg=0.60–0.55), and the glassy groundmass contains feathery augite (mg=0.44). The feathery augite gives a temperature of about 1120°C.

An igneous lithic fragment, which consists mainly of orthopyroxene and augite, occurs in a fayalite-bearing dark clast (D2, α27A). The augite grains (mg=0.87) give equilibrium temperatures of 1230–1270°C, which is similar within the uncertainty of the geothermometer to that for type II ureilitic clasts. The chondrules and chondrites (F) in DAG 319 sometimes contain augite and low-Ca pyroxene. The augite grains in the chondrules give temperatures ranging from higher than 1300 to 1200°C; those in a chondrite (α43A) give about 880°C. A large isolated plagioclase clast (G3, α22A) contains many magmatic inclusions which consist mainly of pyroxene, plagioclase and mesostasis. The pyroxenes are sometimes zoned, from pigeonitic cores (mg=0.84–0.88) to augite rims (mg=0.84.0.89), and temperatures obtained for the augites are 1300–1140°C, similar to the crystallization temperatures of the phenocrysts in the porphyritic felsic clasts (C1).

6.6. Genetic relationships between the major types of lithic clasts

A schematic representation of some possible genetic relationships between the
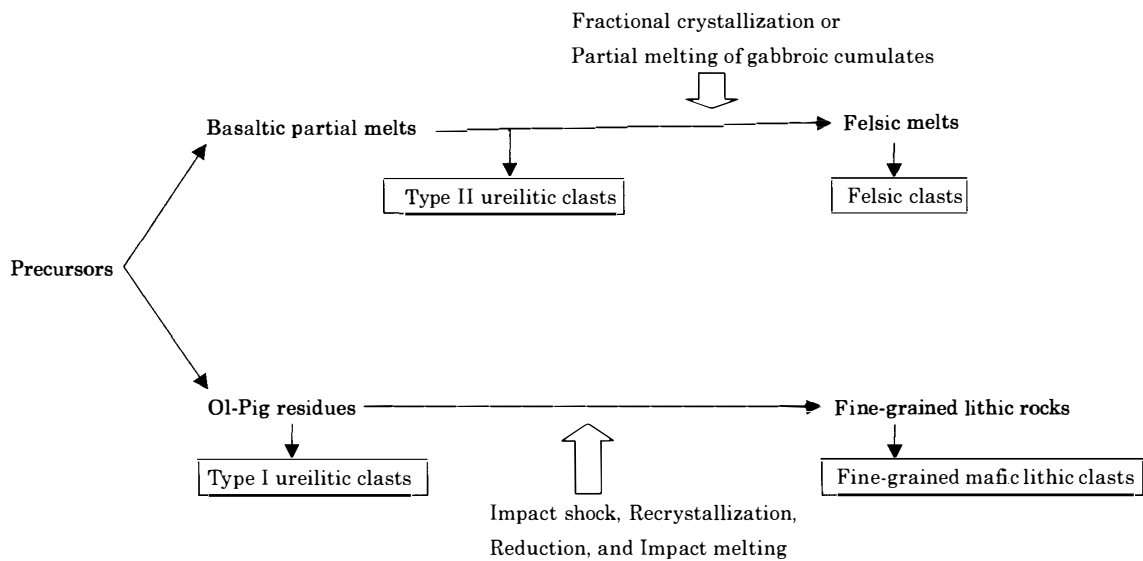
Fig. 17. Genetic relationships between the major types of lithic clasts in the DAG 319 polymict
         ureilite.

major types of lithic clasts in the DAG 319 polymict ureilite is shown in Fig. 17.
This representation is a preliminary but necessary attempt to relate the widely
differing types of lithic clasts in this meteorite. While speculative it does represent
some possibilities that will be further considered.

The precursors of DAG 319 were probably chondritic and experienced partial
melting to produce the Ol-Pig residues and basaltic partial melts (as well as the
metal-sulfide melts, not shown in Fig. 17). The Ol-Pig residues are the type I
ureilitic clasts and the common monomict ureilites. The fine-grained lithic clasts
may have formed from the Ol-Pig residues by intense shock, reduction, and/or
recrystallization.

The basaltic partial melts, which were separated from the Ol-Pig residues
during partial melting, may have first crystallized olivine and pyroxene. An olivine
phenocryst-bearing basaltic fragment and an Ol-Opx igneous fragment, both of
which occur in a Fa-bearing dark clast (D2, α27A), could represent a basaltic melt
and a cumulate, respectively. However, the groundmass of the basaltic fragment
has undergone hydration, as shown above, and the original chemical composition of
the fragment has probably changed.

The basaltic partial melts may have undergone fractional crystallization and
changed their compositions to more felsic melts, and these produced various
cumulates. Some of the cumulates may consist mainly of olivine, orthopyroxene and
augite; these may be the type II ureilites. These cumulates contain many magmatic
inclusions in the olivine and orthopyroxene grains, and their magmatic history can
be traced. Goodrich et al. (1999a, b) concluded that the Hughes 009 ureilite
containing magmatic inclusions must be a cumulate, rather than a residue. Another
type of cumulate contains plagioclase and these may be gabbroic in character. The
fractional felsic melts may have resulted in the felsic lithic clasts (C1). The

important aspect is that no basaltic lithic clasts are found in DAG 319, except for a minor basaltic lithic fragment in a Fa-bearing dark clast. However, felsic lithic clasts are common. An alternative hypothesis for the origin of the felsic lithic clasts is that partial melting of plagioclase-bearing cumulates was involved.

The Fa-bearing dark clasts (D2) include lithic fragments of basaltic and Ol-Opx igneous rocks, as well as Opx-Aug igneous fragments. On the other hand, the Fa-free dark clasts (D1) include felsic lithic clasts. This difference suggests that the Fa-bearing dark clasts (D2) may represent surficial regolithic veneers on the parent body at an early stage of the evolution of the igneous activity, and the Fa-free dark clasts (D1) may represent surficial regolithic veneers at a later stage of evolution.

7. Summary and conclusions

The DAG 319 polymict ureilite contains many kinds of lithic and mineral clasts and essentially all of them have been characterized both mineralogically and petrologically. This was done in order to understand the petrogenesis of the ureilites and their related rock types on the parent body, as well as their shock-modified products and projectile materials. The clasts were classified into seven major groups, from A to G. One major group (A) represents three types of ureilites; the predominant type (type I) which are common monomict ureilites with olivine mg ratios of 0.74–0.84, a rare type (type II) which are unusual monomict ureilites consisting of olivine, orthopyroxene, and augite, with olivine mg ratios of 0.85–0.90, and a third type of magnesian ureilites, with olivine mg ratios of 0.90–0.98 (probably impact-produced). The type II ureilites have magmatic inclusions in their olivines and orthopyroxenes, similar to Hughes 009, and this allows us to determine a portion of the magmatic history of these ureilites. Another very important lithic group consists of the felsic lithic clasts (C) which represent silicate magmas genetically related to the missing basaltic melt components that formed during the formation of the monomict ureilites. The full magmatic history and the petrogenesis of the ureilites will be presented in a future publication. In addition to these two groups, the other two most important groups are the phyllosilicate-rich dark clasts and the chondrules and chondritic fragments. The dark clasts (D) are clearly hydrated, containing not only phyllosilicates but also magnetites (sometimes framboidal clusters) and carbonates (dolomite, magnesite) which can be analyzed for Mn/Cr systematics. These dark clasts will also be analyzed for oxygen isotopic characteristics and will be presented as another publication. The chondrules and chondritic fragments appear to be projectile materials that have produced the DAG 319 regolithic breccia on the surface of the ureilite parent body.

The detailed mineralogical and petrological studies of the DAG 319 polymict ureilite are a necessary first step in deciphering the origin of the ureilites and related materials. Since the details of the wide variety of objects found in this polymict ureilite are so extensive it was decided that the further phases of this study would be presented later.

Acknowledgments

References

Berkley, J. L., Taylor, G. F., Keil, K., Harlow, G. E. and Prinz, M. (1980): The nature and origin of ureilites. Geochim. Cosmochim. Acta, **44**, 1579–1597.

Berkley, J. L., Brown, H. G., Keil, K., Carter, N. L., Mercier, J. C. and Huss, G. (1976): The Kenna ureilite: An ultramafic rock with evidence for igneous metamorphic, and shock origin. Geochim. Cosmochim. Acta, **40**, 1429–1437.

Berkley, J. L. and Jones, J. H. (1982): Primary igneous carbon in ureilites: Petrological implications. Proc. Lunar Planet. Sci. Conf., 13th, Pt. 1, A353–364 (J. Geophys. Res., **87** Suppl.).

Brearley, A. J. and Prinz, M. (1992): CI chondrite-like clasts in the Nilpena polymict ureilite: Implications for aqueous alteration processes in CI chondrites. Geochim. Cosmochim. Acta, **56**, 1373–1386.

Clayton, R. N. and Mayeda, T. (1988): Formation of ureilites by nebular processes. Geochim. Cosmochim. Acta, **52**, 1313–1318.

Davis, A. M. and Prinz, M. (1989): Trace elements in feldspathic clasts in polymict ureilites (abstract). Lunar and Planetary Science XX. Houston, Lunar Planet. Inst., 222–223.

Davis, A. M., Prinz, M. and Laughlin, J. R. (1988): An ion microprobe study of plagioclase-rich clasts in the North Haig polymict ureilite (abstract). Lunar and Planetary Science XIX. Houston, Lunar Planet. Inst., 251–253.

Goodrich, C. A.(1992): Ureilites: A critical review. Meteoritics, **27**, 327–352.

Goodrich, C. A. (1998): A ureilite (Hughes 009) with an unusual shock texture: Implications for the origin of metal in ureilites? Lunar and Planetary Science XXIX. Houston, Lunar Planet. Inst., #1123 (CD-ROM).

Goodrich, C. A., Fioretti, A. M., Molin, G. and Tribaudino, M. (1999a): Primary trapped melt inclusions in olivine in a ureilite–I. Description. Lunar and Planetary Science XXX. Houston, Lunar Planet. Inst., #1026 (CD-ROM).

Goodrich, C. A., Fioretti, A. M., Molin, G., Zipfel, J. and Tribaudino, M. (1999b): Primary trapped melt inclusions in olivine in a ureilite–II. Reconstruction of liquid composition and implications. Lunar and Planetary Science XXX. Houston, Lunar Planet. Inst., #1027 (CD-ROM).

Ikeda, Y. (1999): Petrology of the Asuka-881931 ureilite with special reference to crystallization of interstitial silicate melt. Meteorit. Planet. Sci., **34**, 625–636.

Jaques, A. L. and Fitzgerald, M. J. (1982): The Nilpena ureilite, an unusual polymict breccia: Implications for origin. Geochim. Cosmochim. Acta, **46**, 893–900.

Johnson, C. A., Prinz, M., Weisberg, M. K., Clayton, R. N. and Mayeda, T. (1990): Dark inclusions in Allende, Leoville, and Vigarano: Evidence for nebular oxidation of CV3 constituents. Geochim. Cosmochim. Acta, **54**, 819–830.

Kita, N. T., Ikeda, Y., Prinz, M., Nehru, C. E., Weisberg, M. K., Morishita, Y. and Togashi, S. (1999): *In-situ* SIMS oxygen isotopic analyses of clasts from DAG 319 polymict ureilite (abstract). Antarctic Meteorite XXIX. Tokyo, Natl Inst. Polar Res., 72–74.

Lindsley, D. H. and Andersen, D. J. (1983): A two-pyroxene thermometer. Proc. Lunar Planet. Sci. Conf., 13th, Pt. 2, A887–A906 (J. Geophys. Res., **88** Suppl.).

McSween, H. Y. (1977): Chemical and petrographic constraints on the origin of chondrules and

inclusions in carbonaceous chondrites. Geochim. Comochim. Acta, **41**, 1843–1860.

Miyamoto, M., Furuta, T., Fujii, N., McKay, D. S., Lofgren, G. E. and Duke, M. D. (1993): The Mn-Fe negative correlation in olivines in ALHA77257 ureilite. J. Geophys. Res., **98**, 5301–5307.

Prinz, M., Delaney, J. S., Nehru, C. E. and Weisberg, M. K. (1983) Enclaves in the Nilpena polymict ureilite (abstract). Lunar and Planetary Science XVIII. Houston, Lunar Planet. Inst., 376–377.

Prinz, M., Weisberg, M. K., Nehru, C. E. and Delaney, J. S. (1986): North Haig and Nilpena: Paired polymict ureilites with Angra Dos Reis-related and other clasts (abstract). Lunar and Planetary Science XVII. Houston, Lunar Planet. Inst., 681–682.

Prinz, M., Weisberg, M. K., Nehru, C. E. and Delaney, J. S. (1987): EET 83309, a polymict ureilite: Recognition of a new group (abstract). Lunar and Planetary Science XVIII. Houston, Lunar Planet. Inst., 802–803.

Takeda, H., Mori, H. and Ogata, H. (1989): Mineralogy of augite-bearing ureilites and the origin of their chemical trends. Meteoritics, **24**, 73–81.

Tribaudino, M., Fioretti, A. M., Martignago, F. and Molin, G. (1997): Transmission electron microscope texture and crystal chemistry of coexisting ortho- and clinopyroxene in the Antarctic ureilite Frontier Mountain 90054: Implications for thermal history. Meteorit. Planet. Sci., **32**, 671–678.

Warren, P. and Kallemeyn, G. W. (1991): Geochemistry of unique achondrite MAC 88177: Comparison with polymict ureilite EET87720 (abstract). Lunar and Planetary Science XXII. Houston, Lunar Planet. Inst., 1467–1468.